



Flanders
State of
the Art

16_089_1
FHR reports

Monitoring the morphodynamics of the Zwin inlet

Interim report
1 year after the extension works

DEPARTMENT
MOBILITY &
PUBLIC
WORKS

www.flandershydraulicsresearch.be

Monitoring the morphodynamics of the Zwin inlet

Interim report:
1 year after the extension works

Montreuil, A.L., Dan, S., Verwaest, T.

Legal notice

Flanders Hydraulics Research is of the opinion that the information and positions in this report are substantiated by the available data and knowledge at the time of writing.
 The positions taken in this report are those of Flanders Hydraulics Research and do not reflect necessarily the opinion of the Government of Flanders or any of its institutions.
 Flanders Hydraulics Research nor any person or company acting on behalf of Flanders Hydraulics Research is responsible for any loss or damage arising from the use of the information in this report.

Copyright and citation

© The Government of Flanders, Department of Mobility and Public Works, Flanders Hydraulics Research 2021
 D/2021/3241/287

This publication should be cited as follows:

Montreuil, A.L., Dan, S., Verwaest, T. (2021). Monitoring the morphodynamics of the Zwin inlet: Interim report: 1 year after the extension works. Version 2.0. FHR Reports, 16_089_1. Flanders Hydraulics Research: Antwerp

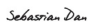

Reproduction of and reference to this publication is authorised provided the source is acknowledged correctly.

Document identification

Customer:	Coastal Division MDK	Ref.:	WL2021R16_089_1
Keywords (3-5):	entrance and inland inlet units; erosion/accretion; hydrodynamics, measurements.		
Knowledge domains:	Hydrodynamics > Current velocities and patterns > In-situ measurements Morphology > Erosion/sedimentation > In-situ measurements		
Text (p.):	48	Appendices (p.):	19
Confidential:	<input checked="" type="checkbox"/> No	<input checked="" type="checkbox"/> Available online	

Author(s):	Montreuil, A-L., Dan, S.
------------	--------------------------

Control

	Name	Signature
Reviser(s):	Verwaest, T.	Getekend door: Toon Verwaest (Signature) Getekend op: 2021-12-16 13:22:00 +01:0 Reden: Ik keur dit document goed 
Project leader:	Dan, S.	Getekend door: Sebastian Dan (Signature) Getekend op: 2022-01-18 11:05:31 +01:0 Reden: Ik keur dit document goed  

Approval

Head of Division:	Bellafkih, K.	Getekend door: Abdelkarim Bellafkih (Sig) Getekend op: 2021-12-16 13:20:20 +01:0 Reden: Ik keur dit document goed 
-------------------	---------------	--



Abstract

The Zwin is a relatively small tidal inlet connected to the North Sea through a tidal channel. The inlet is flooded twice a day and is characterized by the presence of intertidal area with sand banks and salt marshes. From August 2016 until the opening of the dyke in February 2019, large intervention works were carried out to reduce the sediment silting and accretion processes by increasing the amount of water flowing in and out of the inlet (i.e. tidal prism). This project aims to evaluate the success of the intervention work and to improve our understanding on the morphodynamics of the Zwin. Detailed topographic and hydrodynamic measurements were carried out in the entrance and inland inlet units before and after the opening of the dyke. The results indicate significant morphological changes in the entire inlet system where the channel has become deeper and wider. Although a high spatial variability with the onshore mobility of the sandy bedforms occurs in the entrance inlet, the sediment balance is stable there. In contrast, the inland inlet spatially experiences two morphological trends with the dominance of erosion in the middle and east side while accretion takes place westward. Future topographic and hydrodynamic monitoring will allow to monitor further the morphological response and to investigate the contribution of the different driving processes in the Zwin inlet.

Contents

Abstract	III
Contents	V
List of tables.....	VI
List of figures	VII
1 Introduction.....	1
1.1 State of art on inlet morphodynamics.....	1
1.2 Zwin extension : project overview	2
1.3 Zwin project site	4
1.4 Data acquisition and methodology	7
2 Morphodynamics of the tidal inlet.....	10
2.1 Large-scale – entrance and inland inlet (LIDAR).....	10
2.2 Entrance inlet	13
2.3 Inland inlet.....	15
3 Forcing factors	20
3.1 Marine conditions.....	20
3.2 Ad-hoc hydrodynamics in the entrance channel.....	25
3.2.1 Period and conditions of the measurements	25
3.2.2 Locations of the measurements	27
3.2.3 Methodology	30
3.2.4 Results	31
3.2.5 Summary of the ad-hoc measurement.....	41
3.3 Water discharge in the inland inlet	41
4 Discussion	43
4.1 Morphodynamics of the inlet.....	43
4.2 Tidal Prism	43
4.3 Forcing factors in the inlet.....	45
5 Conclusions.....	46
6 References	47
Appendix A	A1
A.4.1. Storming en debiet.....	A5
Appendix B.....	A14
Appendix C.....	A16
Appendix D	A17
Appendix E.....	A18

List of tables

Table 1 – Overview of the interventions in the Zwin	3
Table 2 – Overview of the data timeline from 2017 to 2019.	7
Table 3 – Summary of the characteristics of the Qboat surveys.....	8
Table 4 – Sediment volume in the Zwin inlet units before and after the dyke opening based on the LiDAR surveys.....	11
Table 5 – Summary indicators of the cross-channel based on the RTK-GPS profiles.....	15
Table 6 – Statistic summary of the Qboat DoDs.....	18
Table 7 – Description of the continuous measurement stations.	20
Table 8 – Description of the past storm surges during the period from January to Nov 2019.....	21
Table 9 – Summary of meteo-marine conditions recorded from the stations during the ad-hoc measurement period.	25
Table 10 – Description of the locations and deployment of the instrument frames.....	27
Table 11 – Description of the locations and deployment of the instrument frames.....	27
Table 12 – List of the ad-hoc hydrodynamic measurement settings.	30
Table 13 – List of the ad-hoc hydrodynamic measurement settings.	37
Table 14 – Summary statistics of water discharge across the channel,	39
Table 15 – Statistic summary of the grain size and carbonate content of the three sediment samples collected near the Aquadopps.	39
Table 16 – Statistic summary of the depth-averaged current velocity and direction of the three Aquadopps and Scheur station.....	40
Table 17 – Summary of the debit measurements from Qboat surveys carried out by Aqua Vision.....	42

List of figures

Figure 1 – A) map of the Zwin site two months after the extension, (B) detailed of the main channel and C) topography of the emerged beach and shoreface.....	5
Figure 2 – Long-term morphological trend from section 250 to 255.....	6
Figure 3 – A) Elevation difference between LiDAR survey on 17/04/2018 and Qboat surveys on 13/04/2018, B) elevation difference excluding morphological change below +/- 0.05 m (white areas and C) LiDAR point clouds indicating the absence of data.....	9
Figure 4 – Morphological units of the tidal inlet. Unit delineated based on the 5m contour line.	10
Figure 5 – LiDAR DEMs on A) 06/11/2018 (pre-opening of the dyke), B) 20/04/2019 (post-opening), C) DoD between 06/11/2018 – 20/04/2019 and D) zoom in on the channel.	12
Figure 6 – A) Cross-channel profiles from 2016 to 2019, B) difference of consecutive surveys.....	14
Figure 7 – Qboat DEMs of the inland of the Zwin.	16
Figure 8 – Consecutive Qboat DoDs of the inland of the Zwin.	17
Figure 9 – Qboat DoDs of the inland of the Zwin based on a reference survey on 30/01/2019 (pre-opening dyke).....	18
Figure 10. Extracted profiles from the Qboat DoDs with the pre-opening dyke (01/2019) as reference.	19
Figure 11 – A) Annual wave distribution at Bol van Heist, B) annual current distribution at Scheur for the period from January 2017 to November 2019.....	21
Figure 12 – Time series of water level at Scheur, average wave height, wave direction and wave period at Zwin from 02/2019 to 11/2019.	23
Figure 13 – Average wave (left panels) and current (right panels) distributions per survey periods measured at the coast (currents and waves measured from the Scheur and Zwin buoy respectively) from January to November 2019.	24
Figure 14 – Time series of wind, water level, and currents recorded at the Scheur station and wave parameters at Zwin buoy station during the ad-hoc measurement period.....	26
Figure 15 – Location of the ad-hoc measurement with cross-shore profile (green dots) and Aquadopp sensors (red).	28
Figure 16 – Photographs taken during the deployment of the Aquadopp sensors.	29
Figure 17 – Method of estimating water discharge	31
Figure 18 – Time series of current velocity profile, direction profile, and depth-averaged for the Aquadopp A.	33
Figure 19 – Time series of current velocity profile, direction profile, and depth-averaged for the Aquadopp B.	34
Figure 20 – Time series of current velocity profile, direction profile, and depth-averaged for the Aquadopp C.	35
Figure 21 – Current distributions from the 3 Aquadopps.	36
Figure 22 – Time series of significant wave height (Hm0), period (Tm0) and direction at the Aqd B.	37
Figure 23 – Cross-channel topographic profile with the Aquadopp locations.....	38

Figure 24 – Time series of 30 minutes averaged water level and estimated water discharge across the channel. 38

Figure 25 – Time series of water level, depth-averaged of current velocity and direction of the three Aquadopps and Scheur station..... 40

Figure 26 – Measured water level and discharge before (23/10/2018) and after the opening (16/09/2019).
..... 42

Figure 27 – Hypsometry of the Zwin before (06/11/2018) and after the dyke opening (20/04/2019) as function of water level..... 44

1 Introduction

1.1 State of art on inlet morphodynamics

Along sandy coasts, tidal inlets are common systems, exchanging between the sea and the water basin. Tidal inlet systems are classified into two types depending on their morphology. Primary tidal inlets are characterized by a large delta or channel entrance of several kilometres such as along the Dutch and German Wadden coast and the east coast of USA. Their morphodynamics have been well documented with many identified empirical relationships between geometry and forcings (de Swart and Zimmerman, 2009). Secondary tidal inlet systems (also called 'slufter' in Dutch) connect the sea and the water basin with a small channel. They are present along breached sand bank systems or coastal dunes with a low-lying former beach plain serving as a back-barrier basin (van Bohemen, 1996). The Zwin inlet is a secondary tidal inlet system. Also, they are observed at Slufter on the island of Texel (i.e. a similar morphologic inlet to the Zwin) as well as Zwarte Polder and De Kerf in the Netherlands. The major difference between primary and secondary tidal inlets are the length and width of the basin (100 meters vs kilometres), depth of the inlet (meters vs tens of meters) and the tidal prism (10^5 - 10^6 m³ vs $> 10^7$ m³) (Van der Vegt and Hoekstra, 2012). These have strong implication for their morphodynamic behaviour and evolution. The size and forcing of secondary tidal inlets are similar to the ephemeral inlets or intermittent open-closed inlets and washover systems (Cooper, 2001). Opposed to the primary tidal inlet systems, the secondary ones are subject to larger differences in hydrodynamics and sediment transport during storm versus calm conditions. During calm weather conditions tidal exchange is restricted to the main channel due to the bed elevation, whereas the complete basin is inundated under storm and spring tide conditions. Therefore, there is a large difference in wetted basin between calm weather and storm conditions and truncation of the tidal signal (Lincoln and FitzGerald, 1988). Although extensive research has been carried on primary tidal inlets, the morphodynamics of secondary tidal inlets is still scarce.

In the development process of tidal inlet from formation, maintenance to degeneration, three hydrodynamic forcings are dominant: tidal currents, waves, and storm surge (de Swart and Zimmerman, 2009). They control the direction and magnitude of sediment transport and its divergence resulting in erosion/accretion and thus to the morphology of the seabed and coastline. Morphodynamics consist of complex processes with multiple interactions and feedbacks such as the morphology itself modifies tidal currents and waves which in turn control the sediment transport with constantly changing water levels. Sediment transport patterns and directions are important with respect to tidal inlet development, stability and evolution. In addition, the morphological characteristics of inlets and their relationships with sandy bedforms are controlled by wave energy, tidal range, tidal prism, sediment supply, and rates and direction of sand delivery to the inlets (Fitzgerald, 1996). Bowman (1993) and Hartmann and Bowman (1993) studied the current flow and the intertidal bedforms in the Zwin inlet. They reported the presence of several complex moving sand bedforms characterized by a spatial organization and sediment grain distribution trends reflecting the morphodynamic response to the reversing tidal flow regime. The sediment input into the inlet is mainly caused by tidal asymmetry. The longshore sediment transport also pushes the entrance channel to the east. Previous studies reported that this rate was on average 23 m/yr between 1980-1989 before any human interference (Trouw et al., 2015).

1.2 Zwin extension : project overview

The Zwin is a unique nature reserve situated at the border between Belgium and the Netherlands. The Zwin consists of a small tidal inlet connected to the North Sea through a tidal channel. The inlet is flooded twice a day and is characterized by the presence of intertidal area with banks, mudflats and salt marshes. During high tide, the sea floods the inland area. The water volume in the inlet is variable, depending on the tidal phase and cycle (i.e. neap and spring). Also storm surge further increases the volume of the water exchanged with the sea. The morphology of the tidal channel is controlled by hydrodynamic forcings (waves, tide), local relief and vegetation. In the past, the Zwin inlet was subject to continuous sediment deposition and siltation ranging from 3000 to 40 000 m³/year which was mainly caused by the tidal asymmetry (Houthuys et al., 2013). As a result, areas flooding every tidal cycle were drastically reduced with some locations only inundated during spring tides. Consequently, valuable mudflats and salt marshes were disappearing, along with the native fauna and flora typical for this natural environment.

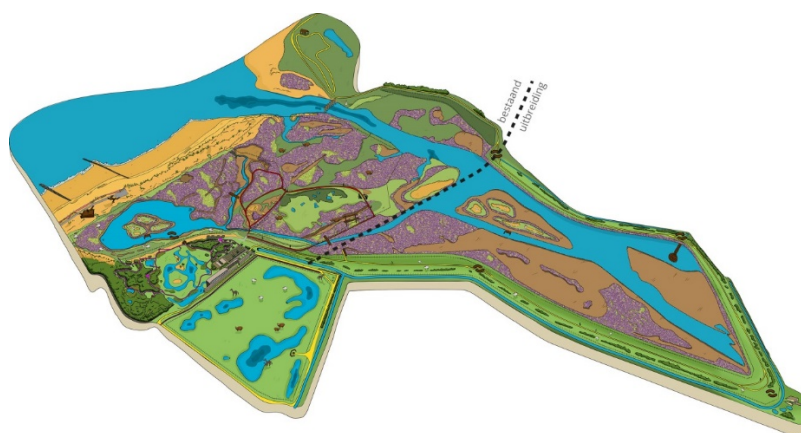
In order to tackle this, large scale intervention works took place in the Zwin from August 2016 to February 2019. These interventions aimed to increase the tidal prism (volume of water that enters and leaves the Zwin channel) by enabling more and faster seawater flow in and out of the channel in order to reduce the silting process. Specifically, the intention of the channel extension was to allow three times as much seawater to flow in and out by increasing the tidal prism up to 1 million m³ (ZTAR Newsletter, 2017). Table 1 presents the final sketch of the Zwin reserve with its doubled surface and lower elevation of some inside areas compared to the pre-intervention work.

Nowadays, the importance of the natural development of coastal ecosystem for multiple functions is recognized (Temmerman et al., 2013). The Zwin extension project aims to develop a sustainable nature management in order to increase the natural dynamism of the inlet system and to restore a number of important types of habitat.

To evaluate whether the interventions achieved the desired objectives and to gain knowledge about the morphological response of the area, it is crucial to monitor the situation of the Zwin system before and after the completed works. The system is composed of several: (i) hydro-morphodynamics, (ii) ecology, (iii) fresh-salt ground water dynamics. In this report, the reported monitoring focuses on the characteristics and changes of the hydro- and morphodynamics of the Zwin area from the pre-opening of the dyke to 8 months after. Data obtained during monitoring are processed, analysed and integrated in order to understand the post-interventions evolution of the tidal inlet.

Table 1 – Overview of the interventions in the Zwin (Source: <http://zwininverandering.eu>)

Year	Date	Intervention
2016	Aug	Excavation work in the Zwin plain and tidal area
	Aug	Part of the pumping station work completed
	Sept till Dec	Excavation of the west dunes
	Sept	Supply of the rubble stones for the embankment of the new dike
	Sept-Oct	Work in the Zwin channel
	Oct	Carry on work on the pumping station in the south of the wharf zone
	Oct	Work for the breeding island and the new dyke
	Nov	Clay cladding started on the dike
	Dec	Extra work on the pumping station
	Dec	Installation of the new pile row in the channel
2017	Feb	Dredged channel in a few weeks Removed Willem-Leopolder
	Mar	Covered the dyke with clay
	Aug	Supply of basalt stones
2018	Jan	Started construction of the pump station
	May	Seed the new dyke for vegetation
	Aug	Work on pump pit and management of Dievegat zone (south of the pump station)
	Aug	Connection between old and new dykes and construction of the dune dyke
	Sept	End of the pump station work Work in Hazegrasduinen and Oosthoek polders (west of Zwin)
2019	28 Jan	Lowering the old dyke
	04 Feb	Opening of the dyke



Zwin tidal inlet after extension.
Surface area extends over 333 ha with 290 ha on Belgian territory and 43 ha in the Netherlands
(ZTAR Newsletter, 2017)

1.3 Zwin project site

The Zwin is a nature reserve designated as Natura2000 site located on the Belgian (west side) and Dutch (east side) borderline in the delta coast (Figure 1). Its inlet constitutes a meandering channel connected to the sea and terminates in the marsh. The Zwin forms a small tidal flood plain, exhibiting a broad range of diverse and well-organized bedforms (e.g. coastal dunes, sand banks/bars, tidal flats and other landforms). The Zwin is a relic of the large estuary in the south of Netherlands that connected the medieval town of Bruges with both a larger fluvial network and the North sea basin. The Zwin inlet was formed by a superstorm in 1134 breaching the Belgian coastline which was then the dunebelt. It remained the south-western most channel of the estuary of the Scheldt river until 1800 (Herrier and Leten, 2010). The size of the tidal flood plain was progressively reduced by land reclamation started from 12th century to 1872 with the construction of the International dyke that embanked the Willem-Leopoldpolder. This caused a reduction of the estuary with a strong sediment deposition and siltation processes favouring the extension of mudflats and saltmarshes. Storms and erosion opened up a new channel and created direct link to the western saltwater pool through an existing small excavated channel (ZTAR Newsletter, 2017). This caused to a major problem of no escape of seawater during ebb phase due to the dam leading to the formation of large pools with small islets. After the restoration work ending in February 2019 with the opening of the dyke, the Zwin covers a surface area > 330 ha, of which 290 ha are located on the Belgian territory. It has an extension of 2.5 km along the coast ad 1.5 km inland from the dune line.

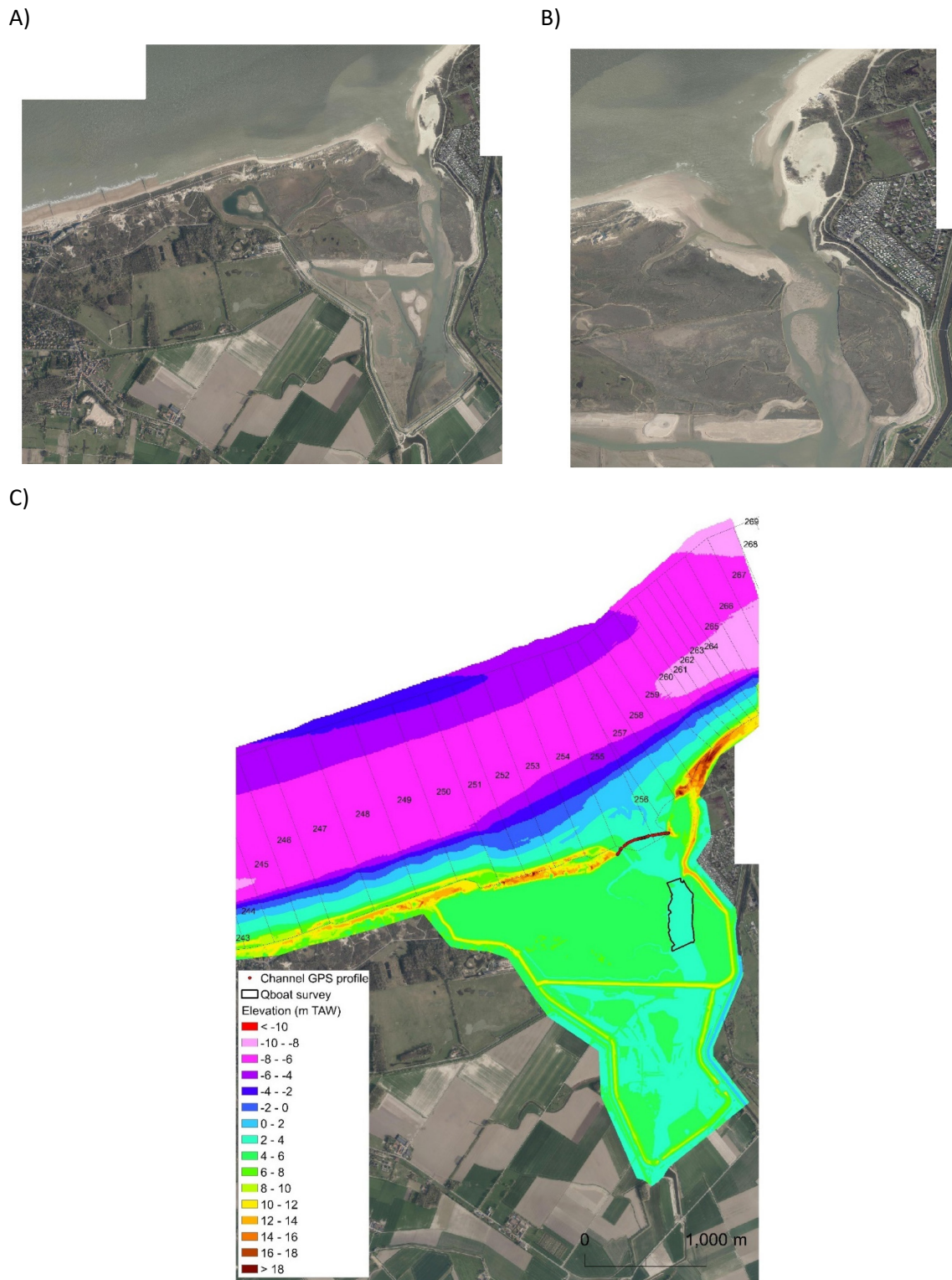


Figure 1 – A) map of the Zwin site two months after the extension, (B) detailed of the main channel and C) topography of the emerged beach and shoreface.

Long-term morphological change of the beach above the low water line (LW) for this coastal stretch (sections 250 to 255) indicate a progressive accretion of $7.47 \text{ m}^3/\text{m}/\text{year}$ during the 2002-2019 period (Figure 2). This was benefited by the frequent beach nourishments in Knokke-Heist and Cadzand carried out in the past. While the sediment balance in the shoreface and adjacent sea bottom (below LW) indicates large fluctuations with an erosional trend of $-15.32 \text{ m}^3/\text{m}/\text{year}$ over the last 10 years. Hydrodynamic processes occurring in the tidal gully Appelzak, about 900 m from the low water line as well as the shallow Paardenmarkt bank situated up to 5 km offshore probably influence the morphological trend of the Zwin sections (Houthuys et al., 2020)

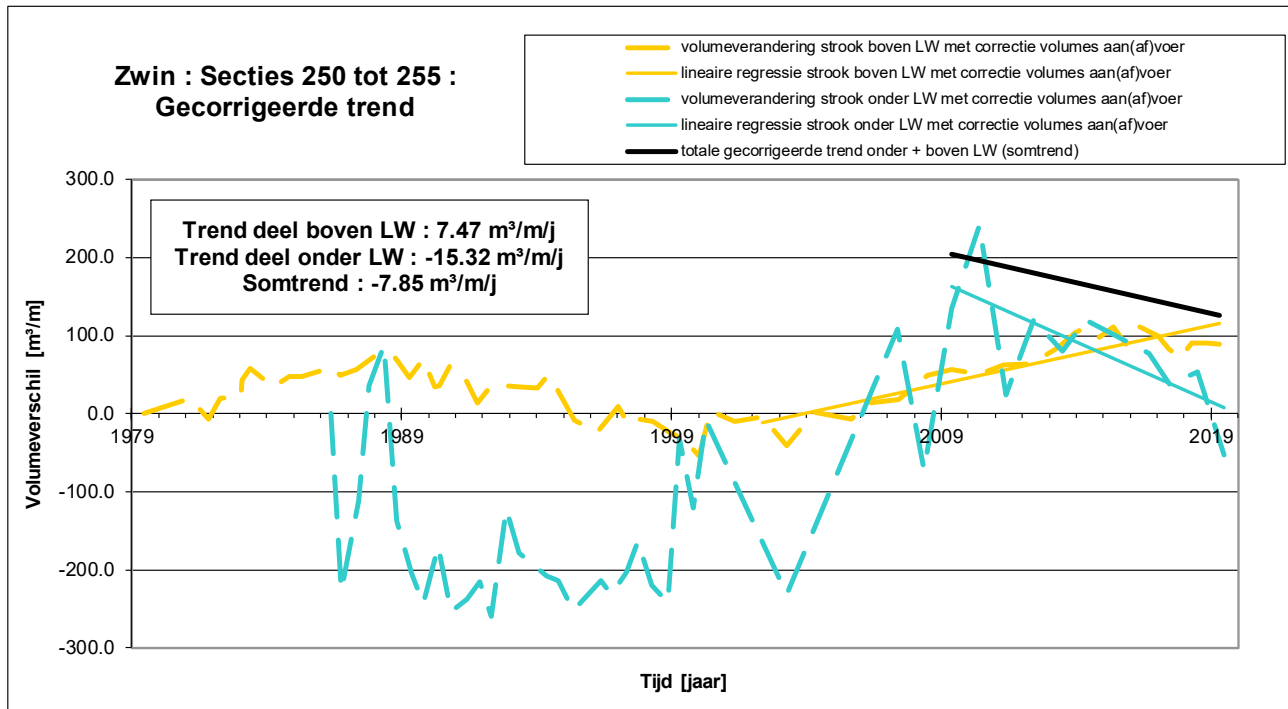


Figure 2 – Long-term morphological trend from section 250 to 255 (Houthuys et al., 2020).

Note: here corrections are applied for sand nourishments, dune excavation and other human interventions in this zone.

At the coast of the Zwin inlet, the tide is semidiurnal and meso/macro-tidal ranging from 3.8 m at neap and 4.7 m at spring condition (i.e. average tide between Zeebrugge and Vlissingen). There is a slight asymmetry as the flood duration is shorter than the ebb duration. The main component of wave energy comes from SW to W. In front of the tidal inlet, the longshore transport of eastward-driven sediment is estimated to be $300\,000 \text{ m}^3/\text{year}$ while the westward transport is three times lower (Bowman, 1993). The Zwin is subject to low wave regime ($< 1.5 \text{ m}$ high) with a period below 6 s. Based on the difference between spring low and high water level, the forcing tide amplitude is of 4.38 m (neap 2.96 m). This is nearly three times greater than the channel depth at the entrance of the inlet. The Zwin channel is thus shallower than the tidal amplitude. Under similar conditions, Lincoln and Fitzgerald (1988) found that the lower part of the flood is bathymetrically truncated causing a shorter flood duration. The tide duration asymmetry improve landward sediment transport and is increased by the interaction with the shallow inlet geometry of the Zwin which lengths ebb duration (Bowman, 1993).

1.4 Data acquisition and methodology

Within the framework of this project a large amount of data is gathered (Table 2). This data set consists of topographic (airborne LiDAR, Qboat, and RTK-GPS profile), hydrological and sediment measurements with several acquisition origins (Coastal Division, Aqua Vision and Flanders Hydraulics Research) and times of acquisition. For their usage an updated data timeline and a coherent storage structure of the data set has been applied to assess the morphodynamics of the Zwin inlet. The presented data timeline was used to analyze and interpret the morphological evolution of the study site, taking into account the information on wave climate and tidal action (forcing factors).

Table 2 – Overview of the data timeline from 2017 to 2019. Note: * LiDAR and Qboat surveys not presented here.

Year	Date	Measurement
2017	17/01	LiDAR*
	02/02	RTK-GPS cross-channel topography
	21-22/02	Qboat flow and bathymetry* (prospection: limited coverage)
	16/05	RTK-GPS cross-channel topography
	26/05	LiDAR*
	10-11-12/07	Qboat flow and bathymetry
	11/08	RTK-GPS cross-channel topography
	12/10	RTK-GPS cross-channel topography
	06/11	LiDAR*
2018	18-19/12	Qboat flow and bathymetry
	08/01	RTK-GPS cross-channel topography
	17/04	LiDAR*
	11-12-13/04	Qboat flow and bathymetry
	09/05	RTK-GPS cross-channel topography
	10-11-12, 16/07	Qboat flow and bathymetry
	23-24-25/10	Qboat flow and bathymetry
	07/11	RTK-GPS cross-channel topography
06/11	LiDAR	
2019	30/01-01/02 (before dyke-opening)	Qboat flow and bathymetry
	06-07/03 (1 month after the dyke-opening)	Qboat flow and bathymetry
	20/04 (2.5 months after)	LiDAR
	17-18/06 (4.5 months after)	Qboat flow and bathymetry
	04/07 (5 months after)	RTK-GPS cross-channel topography
	16-17/09 (7. 4 months after)	Qboat flow and bathymetry

1.4.1. Topography

The morphological change of the Zwin before, immediately and after the opening of the dyke on 04/02/2019 was investigated at large-scale based on the airborne LiDAR surveys. Also, the behaviour of the entrance inlet and inland inlet were assessed using Real-time kinematic positioning (RTK-GPS) profiles and Qboat surveys respectively. The location of the surveys is presented in Figure 1.

1.4.2. Airborne LiDAR surveys

Airborne LiDAR surveys were commissioned along the entire coast by Coastal Division on 06/11/2018 and 20/04/2019. For each survey, the elevation point clouds (x, y, z) were used to generate a Triangulated Irregular Network and then converted to **Digital Elevation Model (DEM)** with 2 m cell size. The cell size was chosen taking into account the spacing between the surveys points (density: > 1 point/m²). Consecutive **DEMs of Difference (DoD)** were calculated from the DEMs, by subtracting the elevations in each grid, on a cell-by-cell basis, in order to visualize the morphological changes after the opening of the dyke.

1.4.3. RTK-GPS profiles

RTK-GPS profiles of the channel entrance was carried out by Coastal Division from 2 to 6 months interval. All the surveys extends from the coastal dunes from the west side of the Zwin to the upper-beach of the Dutch border. In general, the interval between measured points vary less than 1 to 20 m. All the profiles were interpolated with 1 m interval for further analysis.

1.4.4. Qboat surveys

The topography of the inland inlet area was surveyed by Aqua Vision using a remotely-controlled Q-Boat 1800RP system with onboard an ADCP and GPS devices (Appendix A). The advantage of such system is to be capable to sound the bed surface in shallow zones. Nine bathymetric measurements were done from February 2017 to September 2019 with an interval of approximately 4 months. Table 3 describes the characteristics of each survey. The reported error ranges from 2 cm in horizontal and 3 cm in vertical. Regarding the post-processing, the point clouds (x, y, z) were first converted to Lambert72 from ETRS89. Then, they were used to generate TIN and then converted to Qboat DEM with 0.1 m cell size (i.e. appropriate with the spacing between the surveys points). Finally, consecutive Qboat DoDs were calculated from the Qboat DEMs, by subtracting the elevations in each grid, on a cell-by-cell basis.

Table 3 – Summary of the characteristics of the Qboat surveys.

Time	Total point clouds	Processed area (m²)	Meteo-marine conditions
10-11-12/07/2017	265954	95300	SW, NW with medium wind speed (< 8 Bft) Spring tide with high water (HW) of 4.7 m TAW
18-19/12/2017	177942	79478	N, SW of low wind speed HW of 4.6 m TAW
11-12-13/04/2018	175274	77731	NNO, ONO, SW of low wind speed (3 Bft) HW of 4.3 m TAW
10-11-12-16/07/2018	210076	94153	NNW,N from low to medium wind speed Spring tide with HW of 4.7 m TAW
23-24-25/10/2018	223493	94613	W, WNW of medium speed (<6 Bft) Spring tide with HW of 4.8 m TAW
30/01-01/02/2018	157249	79899	SO, O low wind speed (<4 Bft) HW of 3.8 m TAW
06-07/03/2019	89065	49297	S, SW from medium to high wind speed (<7 Bft) Spring tide with HW of 4.4 m TAW Restriction of the survey coverage caused by the occurrence of a storm
17-18/06/2019	214593	95076	NNW, NNO low wind speed Spring tide with HW of 4.5 m TAW
16-17/09/2019	215333	97814	N, NNW medium wind speed (4 Bft) Spring tide with HW around 4.6 m TAW

1.4.5. Assessment of the accuracy of the Qboat surveys

The potential error of the Qboat survey was assessed against LiDAR system by assuming that this latter is a true representative of the inlet topography. The error reported of LiDAR survey is below 0.03 m, however it is likely to be greater when water is still present in the survey zone (i.e. limitation of the laser penetration through water). The LiDAR survey on 17/04/2018 was compared to the Qboat survey on 13/04/2018 (Figure 2, Figure 3). Calm marine conditions occurred during this 4 days period, allowing to compare the two topographic survey systems. The elevation difference is generally below 0.05 m, however it is much larger for the north of the inlet area and along the channel. This is due to the absence or overestimation of the topography from the LiDAR system in areas with the presence of water. In general, this assessment indicates that the error of the Qboat is relatively low in the Zwin inland inlet and thus this topographic system is thus adapted for monitoring such tidal environment.

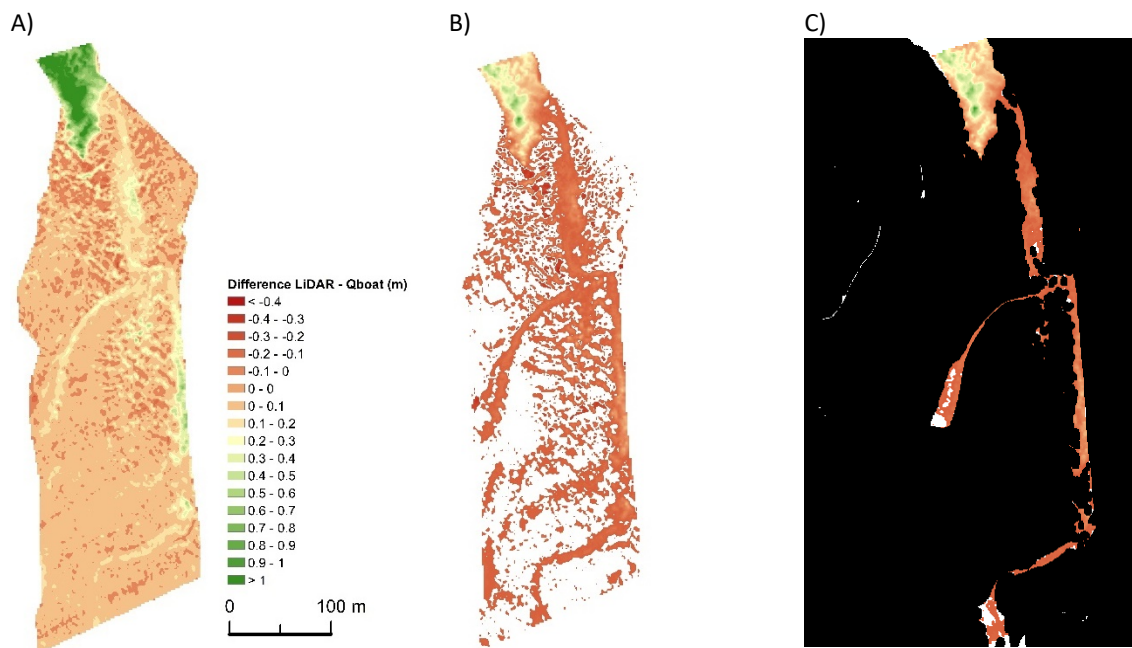


Figure 3 – A) Elevation difference between LiDAR survey on 17/04/2018 and Qboat surveys on 13/04/2018, B) elevation difference excluding morphological change below ± 0.05 m (white areas and C) LiDAR point clouds indicating the absence of data.

2 Morphodynamics of the tidal inlet

The Zwin tidal inlet system is composed of two morphological units (Figure 4). The entrance inlet unit consists of a tidal delta where waves and tides are important constituents of the water motion and sediment transport. In contrast, tidal currents prevail over waves in the inland inlet unit. It is characterized by a main channel undergoing a sequence of bifurcation resulting in a complex patterns of meanders.



Figure 4 – Morphological units of the tidal inlet. Unit delineated based on the 5m contour line.

2.1 Large-scale – entrance and inland inlet (LiDAR)

Figure 5 displays the elevation of the entire Zwin inlet before the opening of the dyke (06/11/2018) and 2.5 months after (20/04/2019) based on the LiDAR surveys. The inlet is composed of a main channel of 1.3 km long from the seaward side of the entrance and the most inland side of the inlet, and it intersects the beach plain back by the Belgian and Dutch coastal dunes. The beach plain is characterized by dynamic sandy bedforms, tidal flats back by salt marshes above 4.8 m TAW. In the entrance inlet unit, the main tidal channel is almost 200 m wide and oriented 130-310° (NW-SE). Its elevation varies from 1.4 m to 3 m TAW from seaward to landward. Noteworthy, these numbers have to be treated with caution due to the limitation of the LiDAR to penetrate water. The sandy bedforms consisting of banks and bars as well as the presence of gullies give a morphological meandering character of the outflow in the channel.

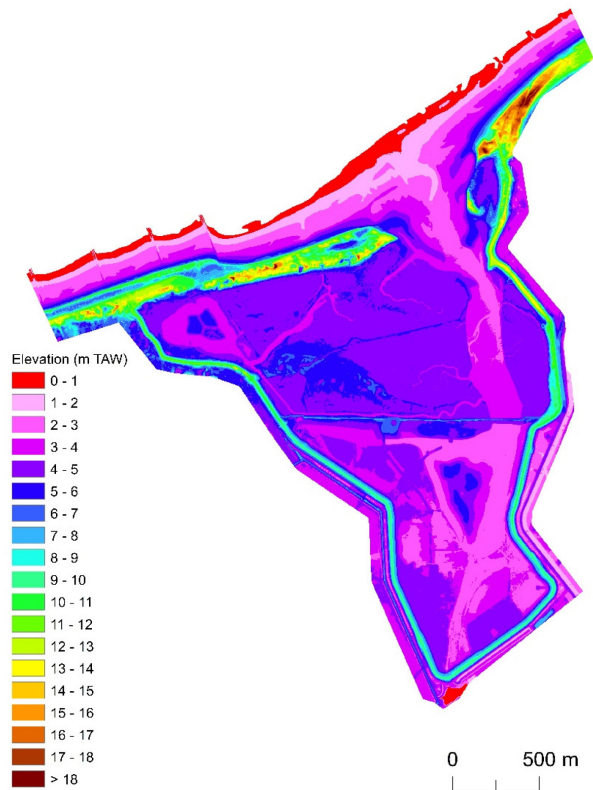
The inland inlet unit is characterized by a main channel oriented 0-180° and is characterized by a width below 100 m and an average elevation of 2.5 m TAW. The channel undergoes a sequence of bifurcations resulting in a complex pattern of meandering channels and tidal flats. This thus leads to spatial variability of the width of the channel.

After 5.5 months, the inland inlet unit was subject to a decrease of sediment volume around 19036 m³ which was equivalent to a reduction in elevation of about 0.18 m (Table 4). The sediment volume in the entrance inlet unit did not change significantly. Significant morphological changes occurred in the main channel which became deeper (>0.2 m) and wider. Erosion reached its maximum of up to -2.3 m located on the edge between the entrance inlet and the inland inlet (around 600 m from the seaward entrance). Also, a spatial variability is observed in the entrance inlet with alternating accretion and erosion zones parallel to the coast and salt marsh line. This footprint is typical of migrating of three dimensional pattern of bedforms. In the inland inlet erosion dominated along the east side of the channel as well as along the edge of the saltmarshes. At the coast, a clear sand accretion took place on the east side (Dutch beach and dunes) contrasting with the variability of the morphological changes of the west side of the Belgian coast. This former might be explained by natural and human interventions with nourishments.

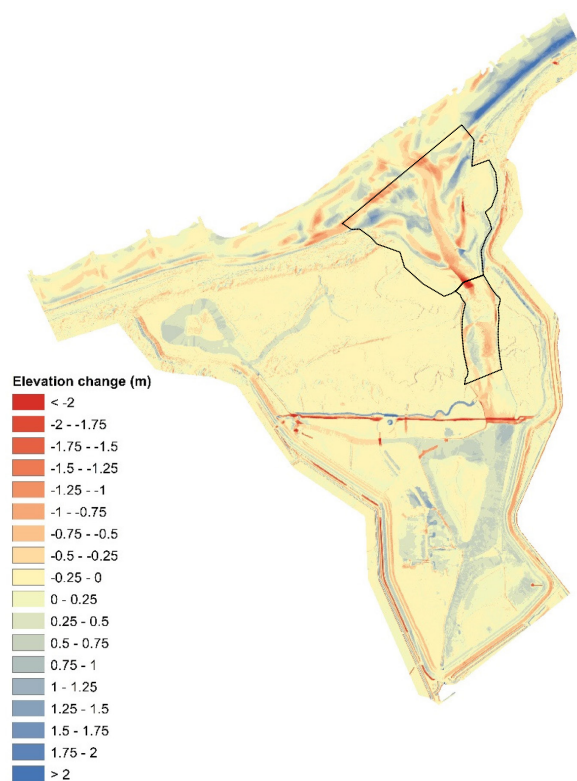
Table 4 – Sediment volume in the Zwin inlet units before and after the dyke opening based on the LiDAR surveys.
Note: Area of the entrance inlet is around 446700 m² and of 107550 m² for the inland inlet

	Volume above 0 m TAW (m ³)	
	Entrance inlet	Inland inlet
06/11/2018	1 749 505.87	343 845.56
20/04/2019	1 747 870.05	324 809.84
Difference (m ³)	-1635.82	-19035.72
Normalized difference (m)	-0.004	-0.179

A) 06/11/2018



C) 06/11/2018 – 20/04/2019



B) 20/04/2019

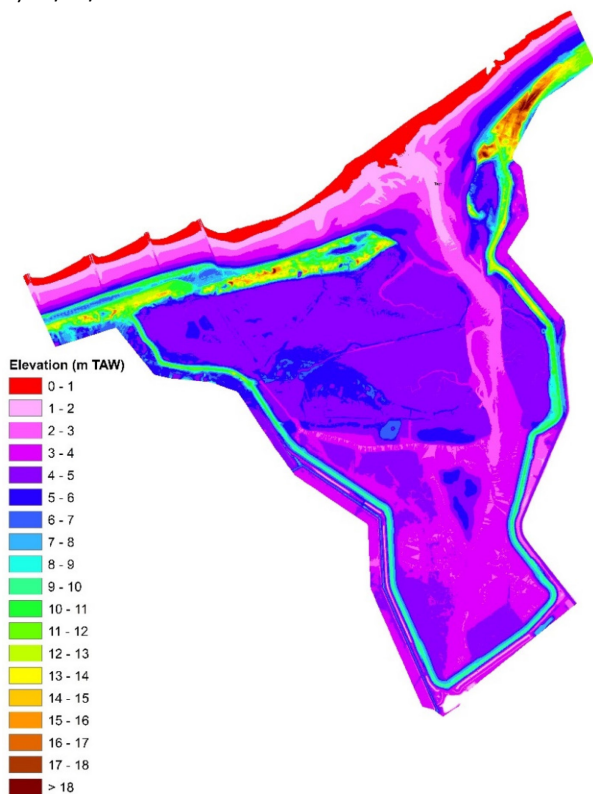


Figure 5 – LiDAR DEMs on A) 06/11/2018 (pre-opening of the dyke), B) 20/04/2019 (post-opening), C) DoD between 06/11/2018 – 20/04/2019 and D) zoom in on the channel.
 Note: the polygons correspond to the entrance and inland inlet units.

2.2 Entrance inlet

The cross-channel morphology of the entrance inlet was investigated based on the RTK-GPS profiles from 08/12/2016 to 04/07/2019. Figure 6A shows the bed elevation as a function of distance from the origin of the profile. A relatively clear morphological change is observed in the main channel located at a distance around 260 and 350 m from the benchmark located in the west dune becoming progressively deep over time. In July 2019, the lowest elevation of the channel was at 1.25 m TAW, while it was at 1.71 m TAW before the opening of the dyke (07/11/2018). The channel became thus 0.46 m deeper in its centre. The largest difference occurred between 07/11/2018 and 04/07/2019 was of 1.1 m (Figure 6B). In addition, the sand bank located from 45 to 160 m with a height up to 6.35 m TAW on 8/12/2016 was totally eroded on 02/02/2017. This is probably due to the excavation work of the tidal area carried out until the opening of the dyke. Then, the sand bank was gradually rebuilt from 11/08/2017. The west dunes seems stable except on 02/02/2017 when excavation work was carried out. In contrast, there is a high variability of the east upper-bank characterized by a sandy tidal flat and low dunes.

Table 5 presents the morphological indicators of the channel extracted from the spring high water (4.7 m TAW) and neap (3.8 m TAW) reference levels. The basin channel based on the spring high water reference on 15/07/2019 was of 87 m³ larger than on 08/12/2016. It reached a maximum volume of 670 m³ on 11/08/2017. A comparable pattern occurred for the width based on the neap high water reference. Also, the width of the channel also followed similar pattern and trend, and it was highly correlated to the basin channel.

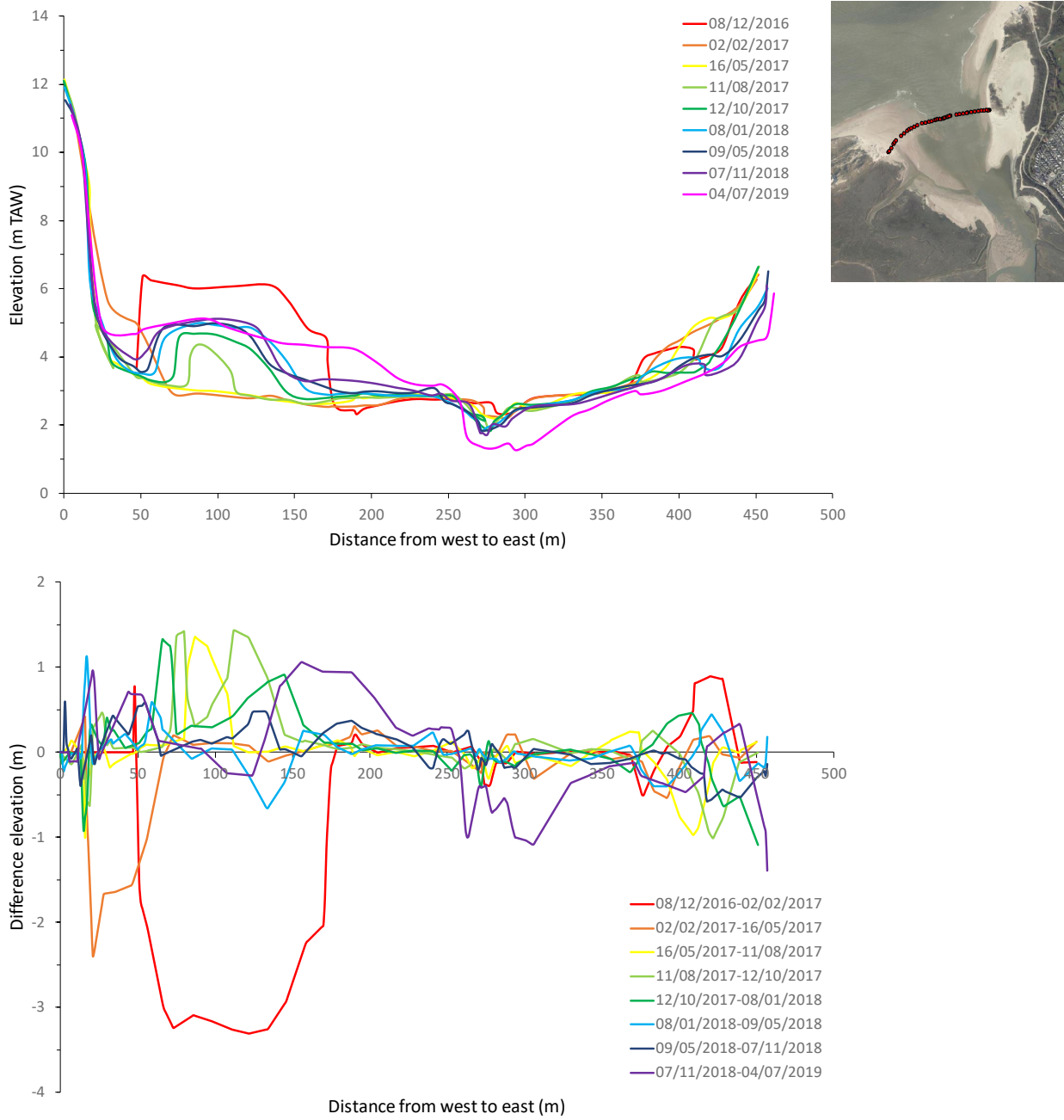


Figure 6 – A) Cross-channel profiles from 2016 to 2019, B) difference of consecutive surveys. Insert: location of the profile measurement. Note: the difference of y-axis. Benchmark is located in the west dune.

Table 5 – Summary indicators of the cross-channel based on the RTK-GPS profiles.

Time	Indicators					
	Basin channel spring (m ³)	Basin channel neap (m ³)	Width spring HW (m)	Width neap HW (m)	Average depth (m)	Minimum depth (m)
08/12/2016	429.74	214.67	268	203	3.10	2.33
02/02/2017	632.13	328.00	359	322	2.94	2.20
16/05/2017	669.84	334.49	384	359	2.91	2.19
11/08/2017	654.69	291.83	396	303	3.05	1.92
12/10/2017	312.80	256.18	347	289	3.25	1.84
08/01/2018	504.32	239.42	312	244	3.09	1.83
09/05/2018	517.65	245.45	325	269	3.11	1.83
07/11/2018	518.50	240.56	322	296	3.09	1.71
04/07/2019	517.03	270.40	340	224	3.18	1.25

2.3 Inland inlet

Figure 7 presents the DEMs, bathymetric maps, from the Qboat surveys in the inland inlet part from 07/2017 to 09/2019. A clear main channel is visible on the east side of the inland inlet which is deeper in the seaward of the inland inlet (<2.5 m TAW) compared to the elevation above 3 m TAW for the rest of the unit. The channel has generally two main meanders in the west side. Large tidal banks up to 3.8 m TAW as well as smaller bars are present along the channel. The consecutive DoDs indicate that the channel gradually became deeper, and in particular in the north of the survey area over the investigated period (Figure 7). In general, the west side of the inlet was subject to slight positive morphological change with the development of sandy banks. While the east side of the inlet eroded and migrated eastward from October 2018 to June 2019. The comparison of the pre- and post-opening dyke bathymetric surveys clear shows that two opposite morphodynamics occurring in the inland inlet with a sediment gain westward, while erosion dominating the east and middle of the survey area (Figure 9). Thus, the channel became deeper up to -2.4 m between January 2019 and September 2019, which corresponded to a decrease of elevation of 0.37 m /month (Table 6). In September 2019, the deepest part of the channel was around 1.2 m TAW.

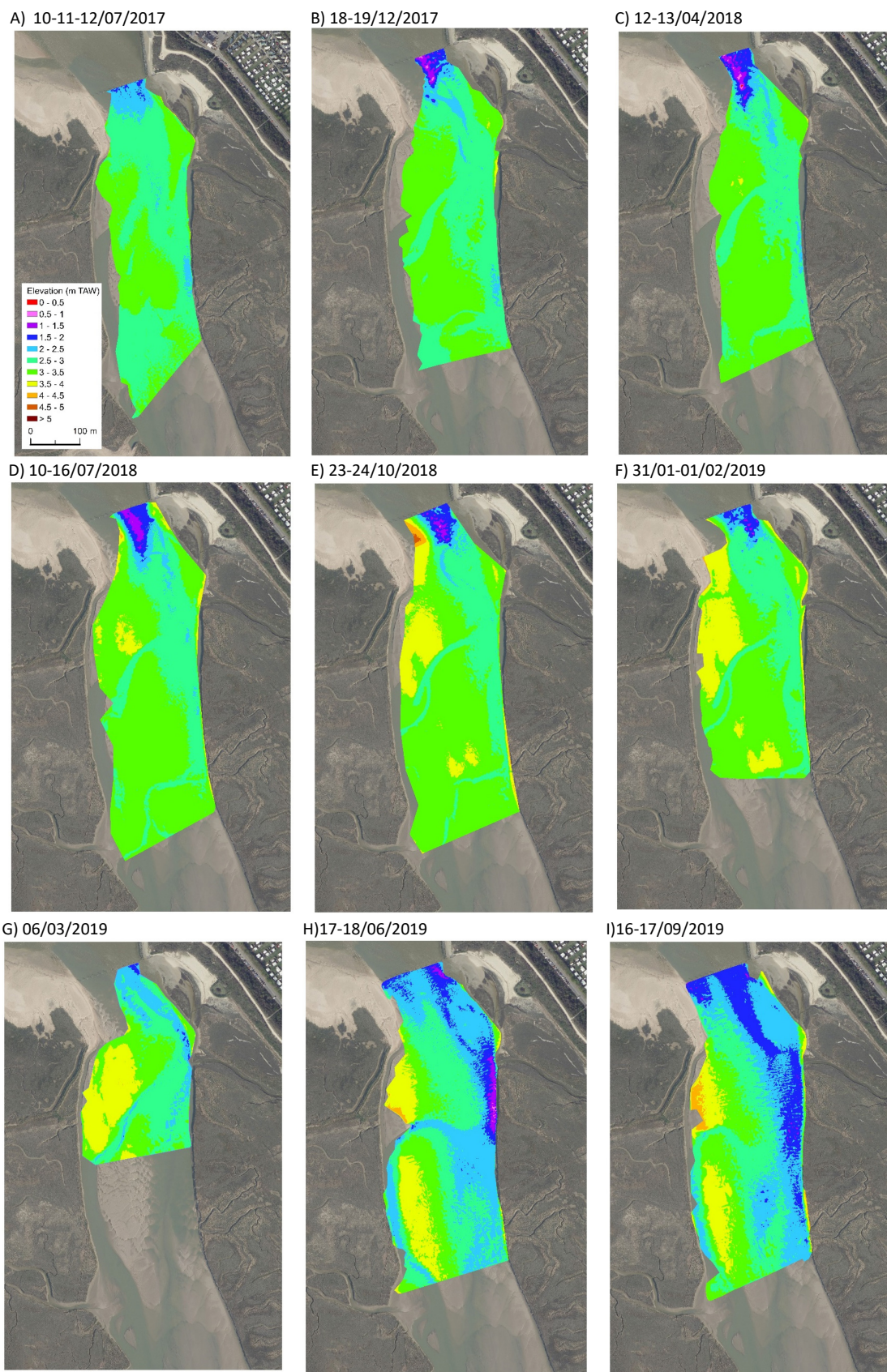


Figure 7 – Qboat DEMs of the inland of the Zwin.

Note: coverage of the surveys varied mainly depending on the meteorological conditions during the data acquisition.

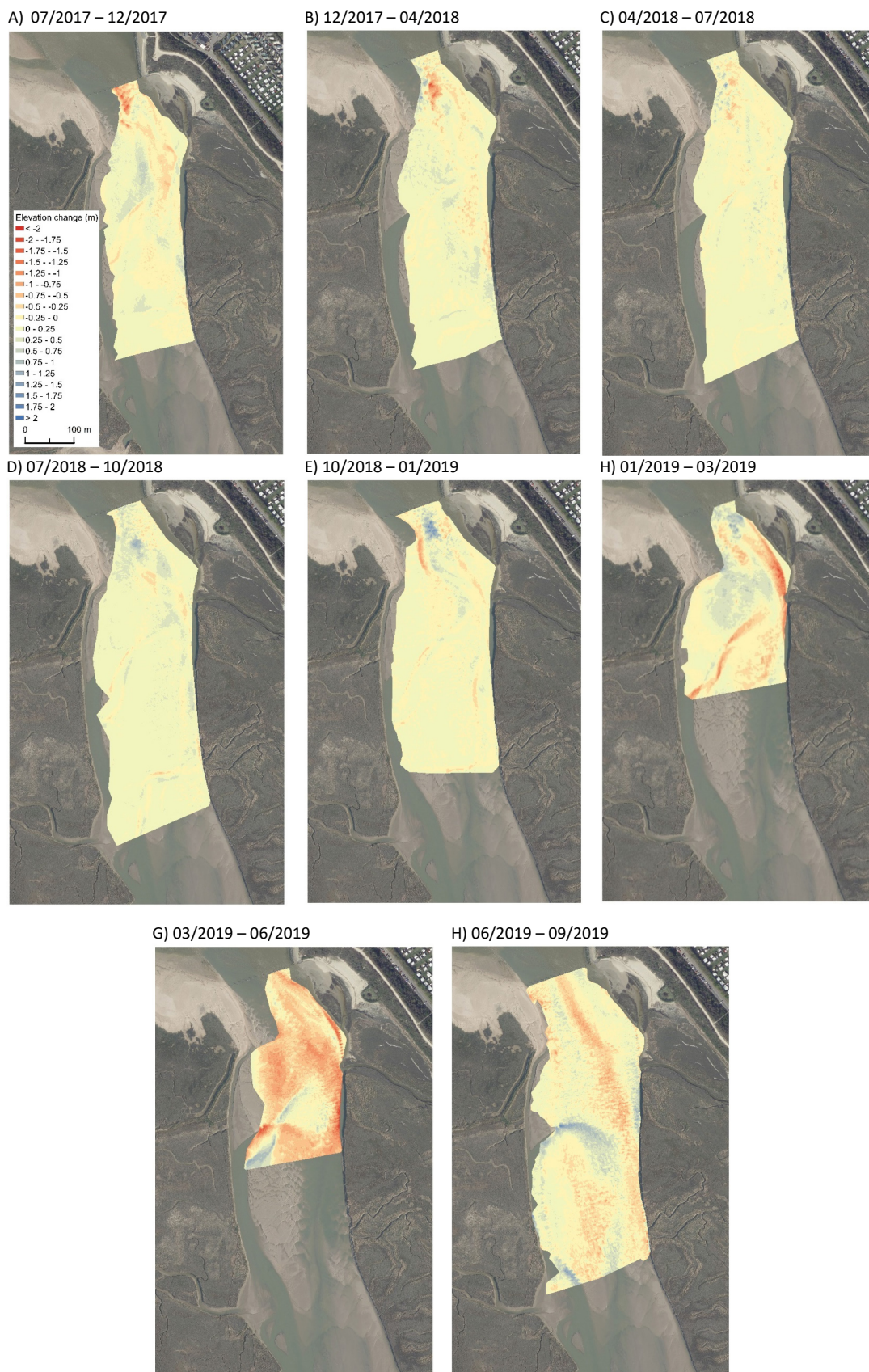


Figure 8 – Consecutive Qboat DoDs of the inland of the Zwin.

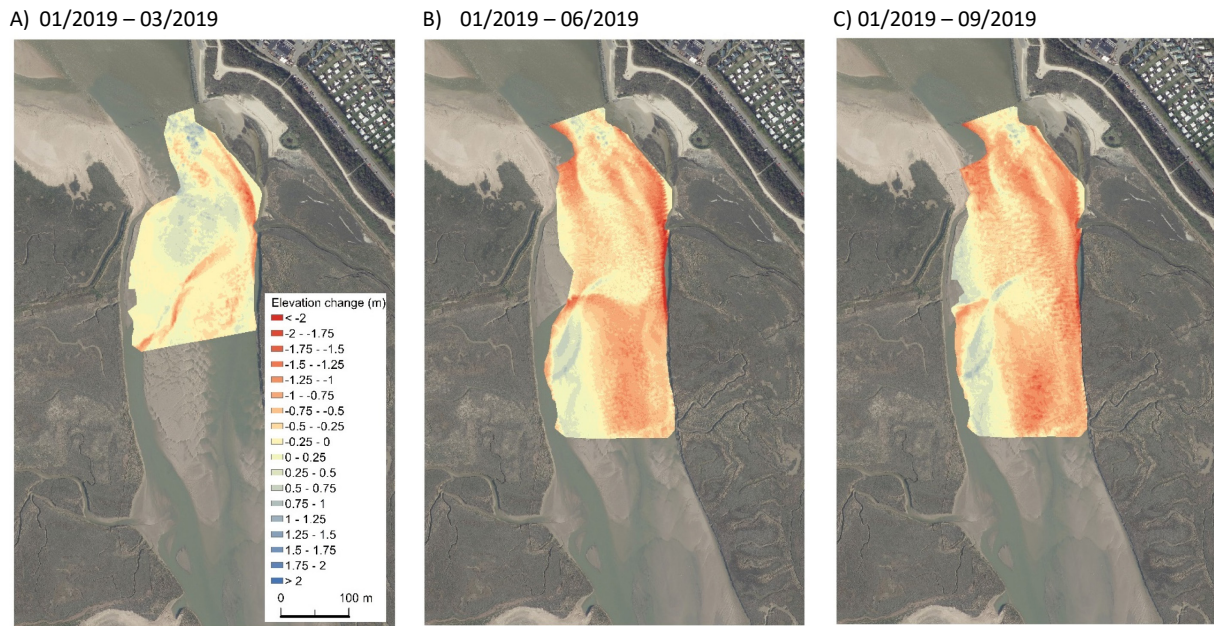


Figure 9 – Qboat DoDs of the inland of the Zwin based on a reference survey on 30/01/2019 (pre-opening dyke).

Results of the four extracted profiles from July 2017 to September 2019 are shown in Figure 10. Appendix B presents the morphological characteristics of the inland inlet extracted from the profiles. Profile 1 located in the seaward of the inland inlet indicates that the bed elevation of the channel became higher and wider there after the opening. The lowest elevation in September 2019 was of 1.6 m TAW, while it was of 0.79 m TAW in April 2018. In contrast Profile 2, 3 and 4 characterized by a large channel width were subject to similar pattern of morphological changes since June 2019 with an increase of depth and in particular to the east side. Therefore, there is a spatial and temporal variability of the channel morphology between the seaward side of the inland inlet unit where the channel is narrow, while the rest features a larger channel width. Decametre mega-ripples, also called submerged dunes, are observed in the channel along the four profiles. These mega-ripples indicate an active sediment transport driven by tidal currents.

Table 6 – Statistic summary of the Qboat DoDs.

DoD consecutive	Difference of elevation (m)			
	Mean	Maximum	Minimum	Standard Deviation
Survey				
07/12/2017	0.01	0.82	-1.80	0.21
12/2017-04/2018	0.04	1.34	-2.07	0.18
04/2018 - 07/2018	0.03	1.56	-1.04	0.12
07/2018-10/2018	0.11	1.30	-0.92	0.13
10/2018-01/2019	0.02	1.89	-1.17	0.17
01/2019-03/2019	-0.04	1.50	-2.06	0.35
03/06/2019	-0.43	1.26	-2.43	0.41
06-09/2019	-0.04	1.81	-1.49	0.30
DoD Ref Jan 2019				
01/2019-03/2019	-0.04	1.50	-2.06	0.35
01/2019-06/2019	-0.46	0.98	-3.06	0.47
01/2019-09/2019	-0.49	1.10	-2.42	0.49

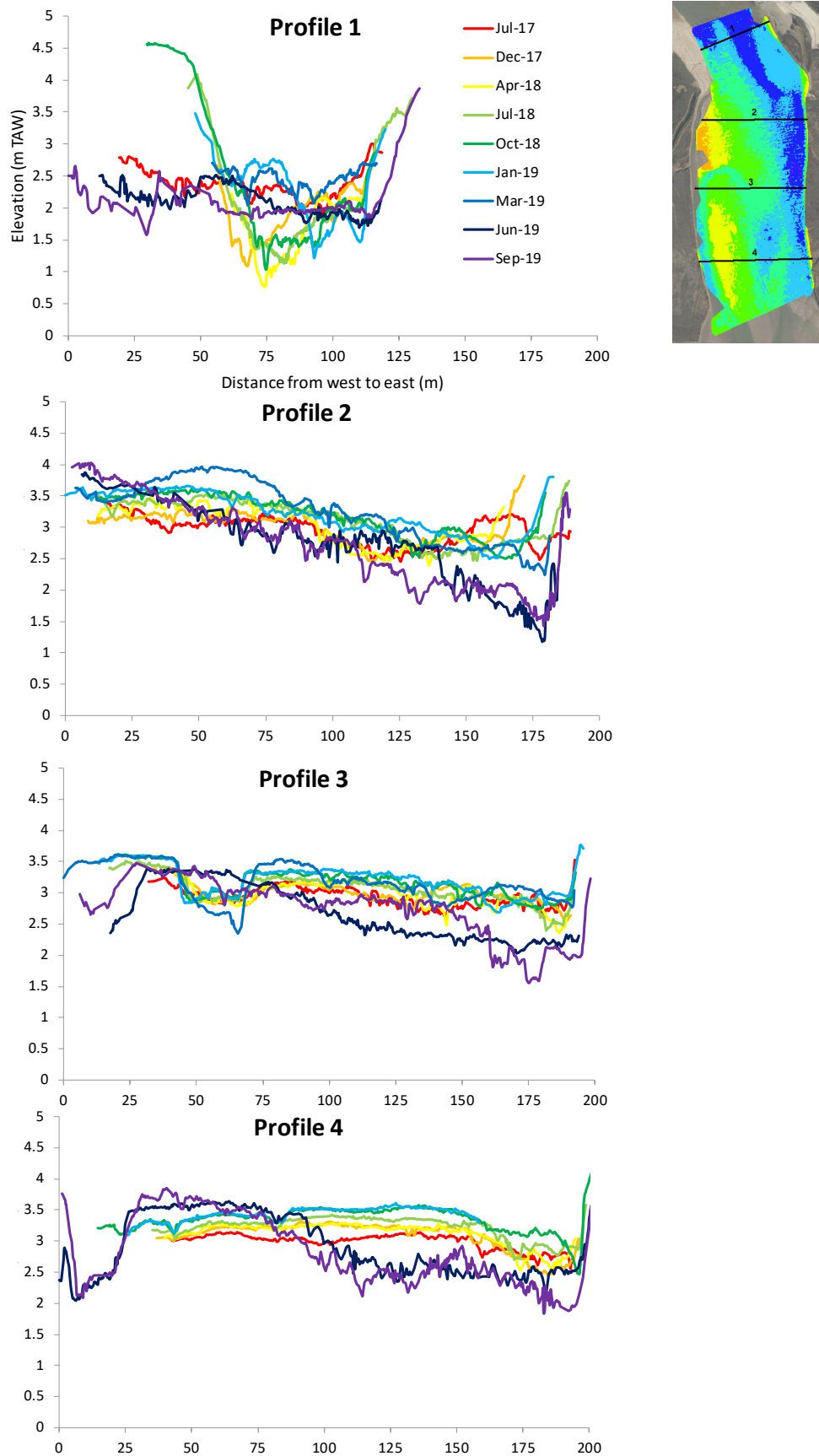


Figure 10. Extracted profiles from the Qboat DoDs with the pre-opening dyke (01/2019) as reference.

3 Forcing factors

3.1 Marine conditions

Water level records with 5 minutes interval were acquired from the wave buoy at Scheur located around 7 km from the study site (Table 7). Additionally, the average wave height, 10% wave height (i.e. comprise the top 10% of the highest waves), period, current velocity and current direction were measured at Scheur from 2017 to 2019. For the recent period (February 2019), the wave parameters (height and direction) were measured at the Zwin wave buoy located around 2 km from the site. Appendix C displays a map of continuous measurement locations.

Table 7 – Description of the continuous measurement stations.

Parameter	Location	Period	Temporal resolution
Water level (m TAW)	Scheur 7km from the study site Depth of - 9.7 m TAW	01/01/2017-06/11/2019	5 min
Wave: -Average wave height (m) -10% highest wave (m) -Average period (s)	Scheur ADCP cell 3 from 3.75m to 6.25m below the water surface	01/01/2017-06/11/2019	From 5 - 30 min
Current: -Velocity (m/s) -Direction (°)	Scheur ADCP cell 3 from 3.75m to 6.25m below the water surface	01/01/2017-06/11/2019	10 min
Wave: -Average wave height (m) -10% highest wave (m) -Period (s) -Direction (°)	Bol van Heist 12 km from the study site at -9.3 m depth	from January 2017 to February 2019	30 min
Wave: -Average wave height (m) -10% highest wave (m) -Period (s) -Direction (°)	Zwin 2km from the study site Depth of - 8 m TAW	22/02/2019-06/11/2019	30 min

Based on the period from 2017-2019, the wave climate is characterized by a mean wave height below 1.5 m for 55% of the time at the coast (Figure 11A). The prevailing waves come from the WSW-W sector. The current velocity at the coast ranges from 0.01 to 1.83 m/s with an average of 0.53 m/s (Figure 11B). The maximum current velocity takes place during the flood tide. Also, there is a velocity asymmetry pattern between the flood and ebb phases mainly oriented eastward and westward respectively. Appendix D presents the time series of forcing factors from 2017 to 2019.

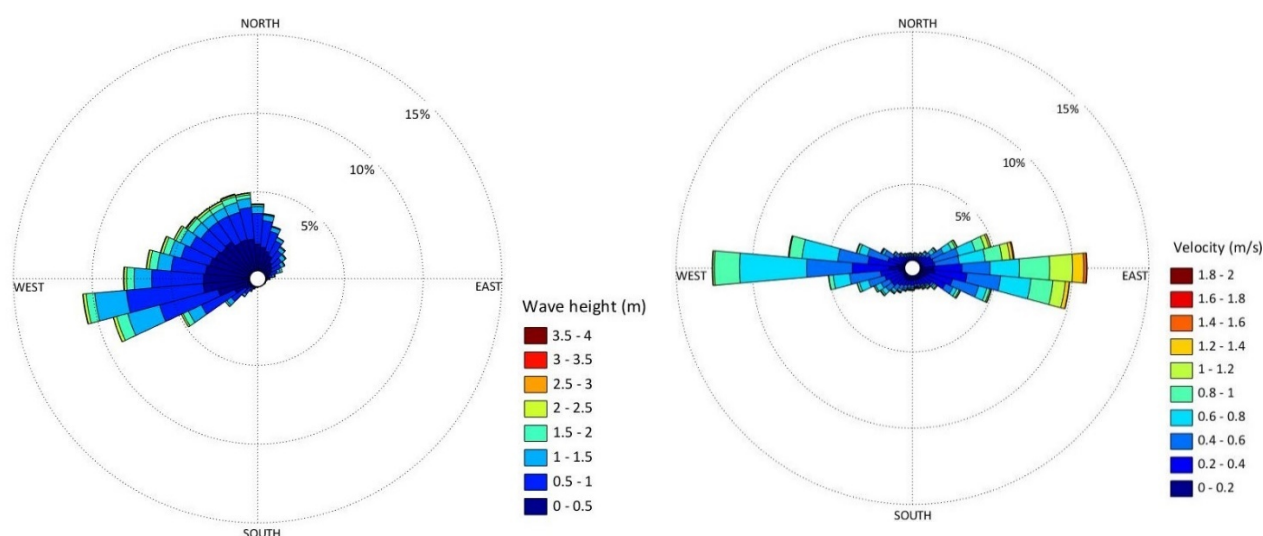


Figure 11 – A) Annual wave distribution at Bol van Heist, B) annual current distribution at Scheur for the period from January 2017 to November 2019. The coastline and the Zwin entrance channel are oriented ENE-WSW (70-250°) and NW-SE (130-310°) respectively.

In total, 5 storm surges were recorded at the coast between January 2017 and November 2019 with two events in 2017, one event in 2018 and two events in 2019 (Table 8). The maximum of water level during these storm surges ranged from 5.30 m to 5.59 m TAW. The largest storm surge happened on 3-4/01/2018 when the high water level was combined with high waves. The average wave height and 10% of highest wave height were of 2.09 m and 2.66 m respectively during this event.

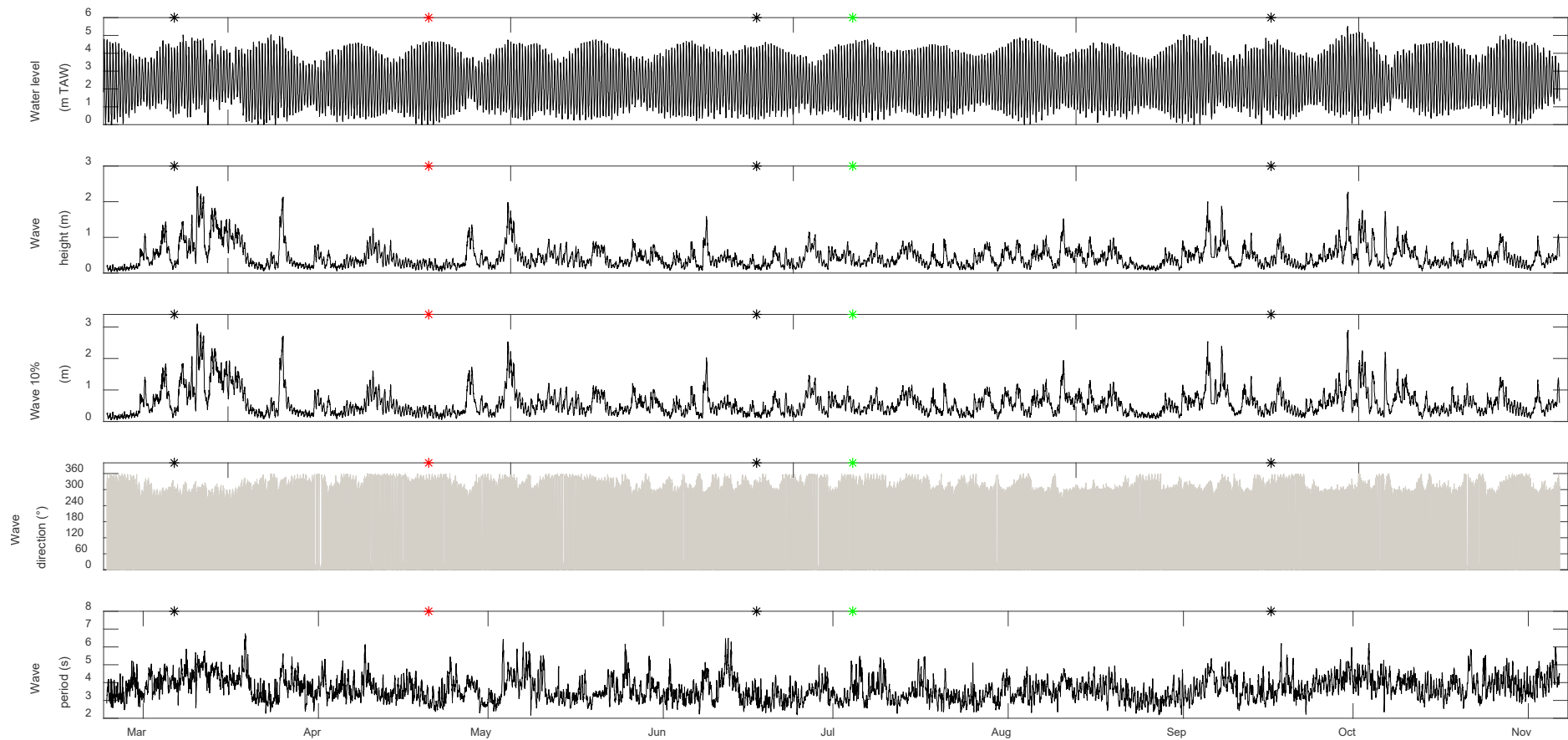
Table 8 – Description of the past storm surges during the period from January to Nov 2019. Data based on Scheur wave buoy.

Storm surge	Maximum water level (m TAW)	Average wave height (m)	10% wave height (m)	Wave period (s)
12-13/01/2017 (peak on 13/01 at 00:25)	5.40	2.29	2.96	5.06
08/12/2017 (peak at 03:40)	5.30	1.82	2.16	4.71
03-04/01/2018 (peak on 03/04 at 12:50)	5.59	2.61	3.35	5.11
08/01/2019 (peak at 14:25)	5.39	2.68	3.42	5.69
30/09/2019 (peak at 01:00)	5.51	2.09	2.66	4.51

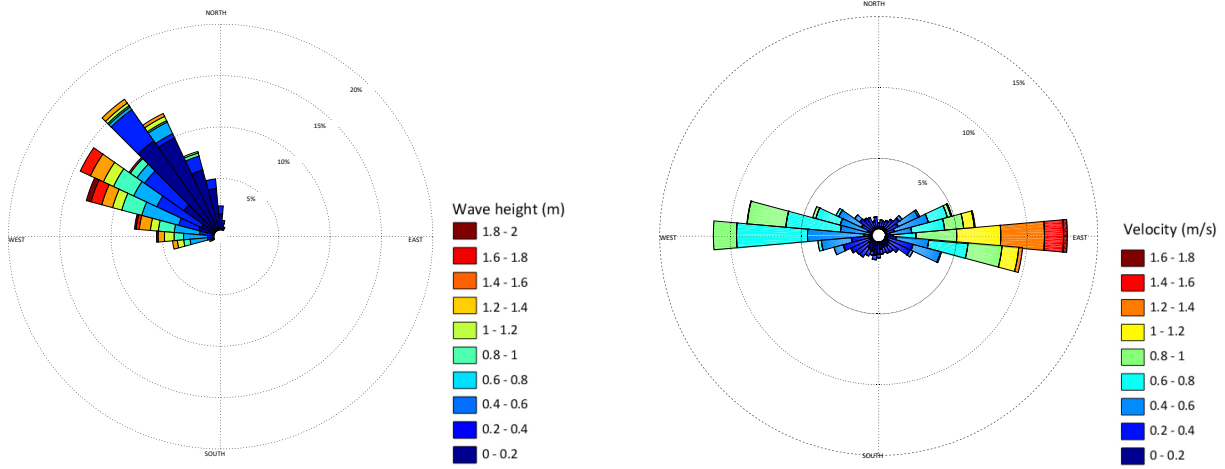
To evaluate the morphodynamics of the Zwin inlet before and after the opening of the dyke, it is necessary to analyse the forcing conditions over this period from 02/2019 to 11/2019. The average wave height ranged from 0.04 to 2.43 m with a mean of 0.46 m over this period at the Zwin buoy (Figure 12). Also, the top 10% waves were below 1 m for 88% of the time. The waves mainly came from 300-360° (NW - N) and they were characterized by a period of 3.7 s. Figure 13 presents the wave and velocity current distribution between the Qboat surveys just before and after the opening of the dyke. From 30/01/2019 to 17/09/2019, the waves were mainly coming from the sector 280-360° (W-N). The period from 30/01/2019 to 07/03/2019 was relatively energetic with wave height above 1 m for nearly 10% of the time. The maximum wave height was of 1.44 m. The most energetic period was from 07/03/2019 to 18/06/2019 when high waves above 2.40 m were recorded. This happened on 10/03/2019 at noon when the waves exceeded 2 m for 4 hours and the

water level reached 4.80 m TAW. Calm conditions occurred from 17/06/2019 to 17/09/2019 (summer) when the mean of wave height was of 0.44 m. The velocity current roses indicate similar regimes between the three periods with an average of 0.5 m/s. High velocity currents above 1.4 m/s occurred during flood phase directed to the east, while up to the westward ebb currents is below 1 m/s most of the time. The highest current of 1.74 m/s was recorded 1 hour before high tide. This was probably the combination of tide and meteorology driven currents directed eastward.

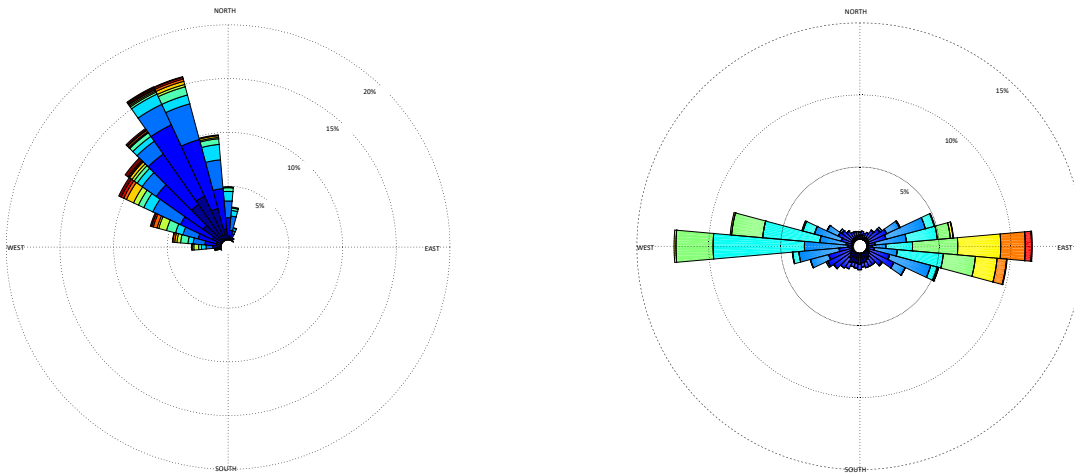
Figure 12 – Time series of water level at Scheur, average wave height, wave direction and wave period at Zwin from 02/2019 to 11/2019. Black, red and green stars correspond to the LiDAR, RTK-GPS and Qboat surveys respectively.



30/01-01/02/2019 – 06-07/03/2019



06-07/03/2019 – 17-18/06/2019



17-18/06/2019 – 16-17/09/2019

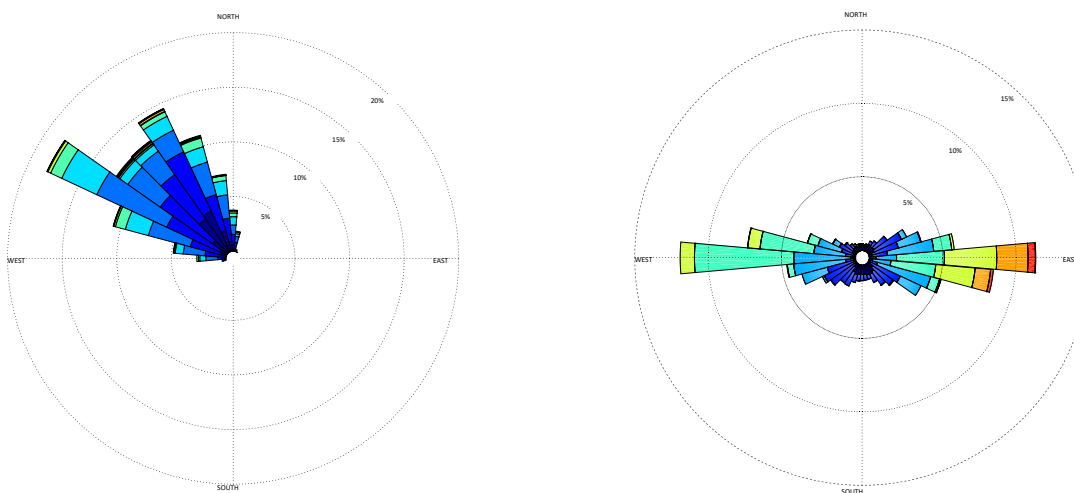


Figure 13 – Average wave (left panels) and current (right panels) distributions per survey periods measured at the coast (currents and waves measured from the Scheur and Zwin buoy respectively) from January to November 2019. The coastline and the Zwin entrance channel are oriented ENE-WSW (70-250°) and NW-SE (130-310°) respectively.

3.2 Ad-hoc hydrodynamics in the entrance channel

In-situ ad-hoc measurements were carried out by FHR in the Zwin inlet on 04-05/07/2019. The objectives are to determine the hydrodynamics during spring and calm condition and also to estimate the characteristics of the water discharge across the channel.

3.2.1 Period and conditions of the measurements

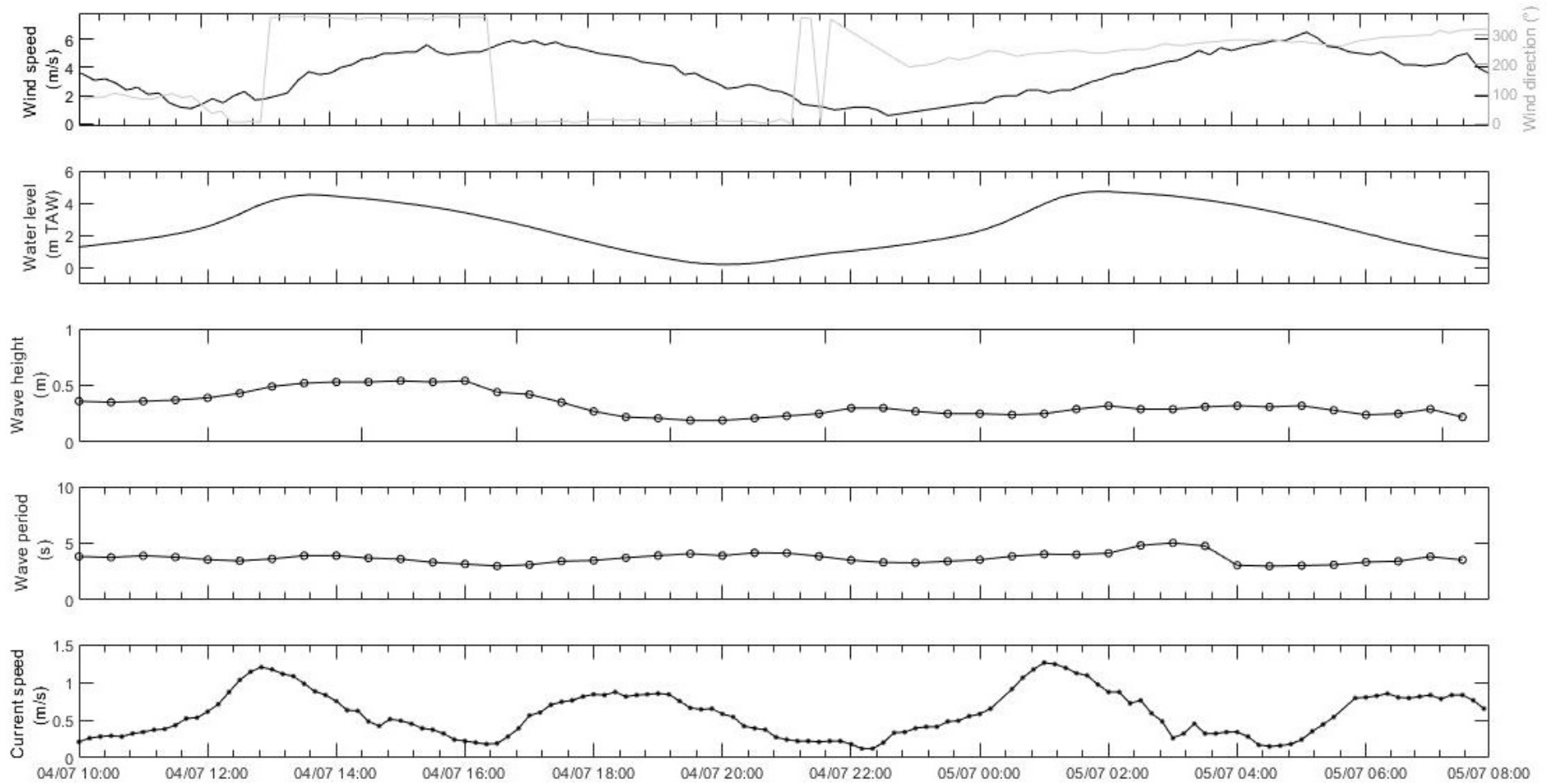
Meteo- and marine conditions were recorded from the continuous offshore stations at Scheur and Zwin located around 7 km and 2 km respectively from the study area (Appendix A). The ad-hoc measurements were carried out from 04/07 at 10:00 UTC (all deployed sensors at 9:00) to 05/07/2019 at 8:00 (all retrieved sensors at 9:00) during a spring tide period. The total duration of the measurement was of 22 hours.

Figure 14 and Table 9 present the recorded meteo-marine data at Scheur and Zwin buoy (Source: Meetnet) during the ad-hoc measurement period. Fair weather conditions occurred with the average wind of 3.61 m/s coming from NNE in the beginning of the measurements to turn to SW-WSW from 4/07 at 22:00. The average wave height was of 0.33 m with a maximum of 0.54 m at the Zwin buoy. High tide happened on 04/07 at 13:35 and 05/07 at 1:50 with a water level reaching 4.53 m and 4.73 m TAW respectively at the Scheur station. There, the current velocity ranged from 0.12 to 1.26 m/s with an average of 0.55 m/s.

Table 9 – Summary of meteo-marine conditions recorded from the stations during the ad-hoc measurement period.

Parameter	Location	Condition
Wind speed	Scheur 7km from the study site measuring at 10m high	Avg: 3.61 m/s Max: 6.50 m/s
Wind direction	Scheur 7km from the study site	Avg: 193° Max: 360°
Water level	Scheur 7km from the study site Depth of - 9.7 m TAW	High tide 1: 4.53 m on 4/7 at 13:35 High tide 2: 4.73m on 5/7 at 1:50 Low tide 1: 0.22 m on 4/7 at 19:55 Low tide 2: sensor removed before
Wave	Zwin (ZHG) 2km from the study site Depth of - 8 m TAW	Avg: 0.33 m Max: 0.54 m
Currents	Scheur ADCP cell 3 from 3.75m to 6.25m below the water surface	Avg: 0.55 m/s Max: 1.26 m/s

Figure 14 – Time series of wind, water level, and currents recorded at the Scheur station and wave parameters at Zwin buoy station during the ad-hoc measurement period.



3.2.2 Locations of the measurements

The location of the deployed 3 sensors and the measured cross-channel topographic profile is presented in Figure 15. Location of the ad-hoc measurement with cross-shore profile (green dots) and Aquadopp sensors (red). Figure 15 (see Table 10 for further description). The Aquadopps were dug into the sand using a krinner mounting screw or a drill mounting construction (Figure 16). An orange rope was fixed on each structure to facilitate the instruments retrieval.

Table 10 – Description of the locations and deployment of the instrument frames.

Sensor	Coordinates	Elevation (m TAW)	Description of the location
Aquadopp A (Aqd A)	80304.434E 229170.35N	1.59	in the deepest part of the channel
Aquadopp B (Aqd B)	80330.276E 229186.221N	1.72	east side of the bank of the channel
Aquadopp C (Aqd C)	80386.548E 229213.691N	2.87	in a little puddle, east side of the channel

Table 11 indicates the convention used for the measurements.

Table 11 – Description of the locations and deployment of the instrument frames.

Item	Convention
Coordinates	Lambert72
Elevation	m TAW
Time	UTC
Current velocity	m/s
Current direction	Degree relative to North
Wave height	m
Discharge	m ³ /s



Figure 15 – Location of the ad-hoc measurement with cross-shore profile (green dots) and Aquadopp sensors (red).

Aqd A



Aqd B



Aqd C



Figure 16 – Photographs taken during the deployment of the Aquadopp sensors.

3.2.3 Methodology

Currents

Description: Three Aquadopp profilers were used to measure the current velocity and direction in multiple layers through the water column. They measured flow velocities in three directions: eastward, northward and vertical.

Principle of operation: The Aquadopp sensor measures flow in a set of cells along three acoustic beam pointing in different directions to obtain the current profiles using the acoustic Doppler effect technology (i.e. based on difference of transmitting a short pulse of sound and receiving its echo). The blanking is the distance between the instrument transducers and the closest control volume (layer) within which no measurement takes place was around 0.2 m. The function of the blanking zone is to allow for a Doppler shift the signal travelling until the closest layer. All the Aquadopp sensors were set-up in Normal mode. Table 12 summarizes the Aquadopp settings.

Heading, Pitch and roll: The three sensors were stable with generally limited heading, pitch and roll motions of less than 4° which are acceptable.

Related software and output files: The data were processed using Storm software (Nortek) and contain velocity and direction currents on the two horizontal and vertical directions for each cell through the water column, as well as tilt, pressure, sea temperature and other sensor characteristics.

Waves

Description: Wave height, period and direction were measured using the Aquadopp B sensor.

Principle of operation: The sensor is set-up in wave bursts which is sequential mode (i.e. the system first collects a current profile, then wave data for a period of time determined by the number of samples and the sampling rate). Wave measurements is also based on the Doppler effect principle.

Related software and output files: The data retrieved contain information about wave parameters. Data processing was carried out with Storm software. Data measured time is in winter time.

Table 12 summarizes the ad-hoc hydrodynamic measurement settings.

Table 12 – List of the ad-hoc hydrodynamic measurement settings.

Sensor	Measurement	Profile interval (s)	Average interval (s)	Cell size (m)	Blanking distance (m)	Sampling frequency
Aqd A	Current	60	60	0.1	0.2	
Aqd B	Current	120	60	0.1	0.2	
	Wave	3600		0.5	0.2	2Hz
Aqd C	Current	60	60	0.1	0.2	

Cross- channel topography

A cross-channel topographic profile was carried out along the monitoring profile on 04/07/2019. It was collected by MDK using a Real-time kinematic (RTK-GPS) system.

Estimation of water discharge

Water discharge was estimated by dividing the cross-channel topographic profile in 4 sections to calculate the water area (A_{water}) (Figure 17). Method of estimating water discharge. For this, the estimated geometric area (A_{geo}) was subtracted from the core area (A_{core}) for each section. Then, the water discharge per section was calculated by multiplying A_{water} and the depth-averaged velocity current measured by the Aquadopps for the respectively section. Finally, the water discharge of the four sections was summed. Cross-channel topographic profile was interpolated with a distance interval of 0.1 m to extract representative water level. Also, the depth-averaged velocity current and water level was averaged every 30 min for the campaign period. It was assumed that the current velocity measured by the Aquadopps at a specific location is representative of the velocity for the entire section while it is likely to be lower near the embankment of the channel.

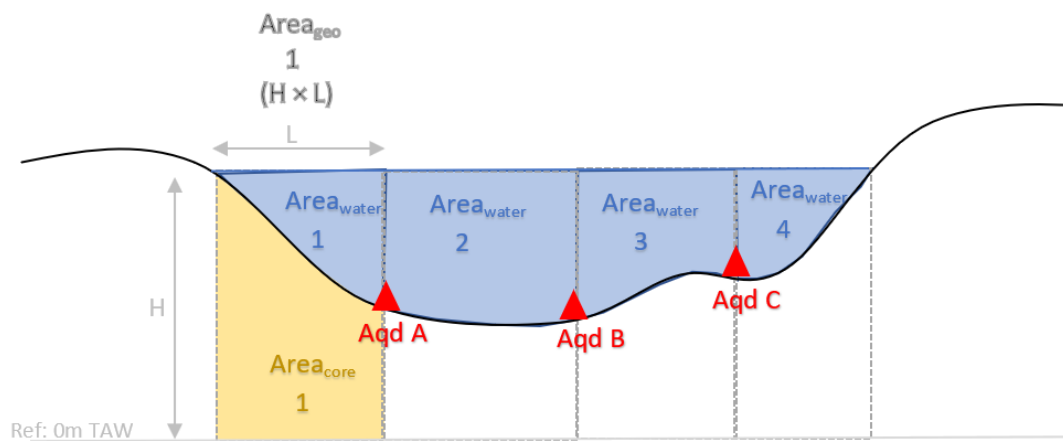


Figure 17 – Method of estimating water discharge

Sediment

Sub-layers sediment samples were collected near the three Aquadopps. Grain size and carbonate content were analysed in the laboratory.

3.2.4 Results

Current characteristics

Time series of current velocity profile, direction profile, and depth-averaged of the Aqd A in the deep channel, Aqd B at the embankment, and Aqd C in the east puddle are shown in Figure 18, Figure 19 and Figure 20 respectively.

The average current velocity was of 0.54 m/s for Aqd A and Aqd B and of 0.21 m/s for Aqd C. This suggests that the current in the deep channel was as fast as near the embankment. While it was two times lower in the shallow puddle. The maximum current velocity reached 1 m/s for both Aqd A and Aqd B sensors and 0.69 m/s for Aqd C. In general, the highest current velocity were measured 30-40 minutes before high tide. A drop of velocity occurred 30 minutes after high tide for the three Aquadopps, but then gradually increased during mid-tidal phase. One hour before low tide, the current velocity was below 0.5 m/s for Aqd A and B and 0.14 m/s for Aqd C. During low tide periods, the instruments were dry or have a thin water layer on top, therefore the measurements on these periods were removed from the analysis.

Regarding the direction, the current in the channel was driven to SSE (150-160°) during the flood phase. A sudden shift of direction to NW (330-340°) occurred when the current velocity drops 30 min after tide and the ebb phase. In contrast, the current direction measured by Aqd B at the embankment was orientated from ENE (60-70°) and SW (230-240°) during the flood and ebb phase respectively. Although the topography of the channel embankment might force current to deviate its direction, this abrupt shift of direction between the tidal phases looks suspicious. Further measurements need to confirm this possible explanation, but this is more likely caused by the iron screws used to set-up AqdB which magnetically influenced the compass sensor. Although there is some directional variability in the measurements of Aqd C due to probably some local currents generated by wind in the puddle, the flood and ebb phase was generally dominated by ESE direction (120°) and SW (200-240°) respectively, similar orientations to Aqd A.

Appendix D displays the current velocity for the three components (u (East), v (North), z (Up)) for cell 1 of the three Aquadopps.

Aqd A – deep channel

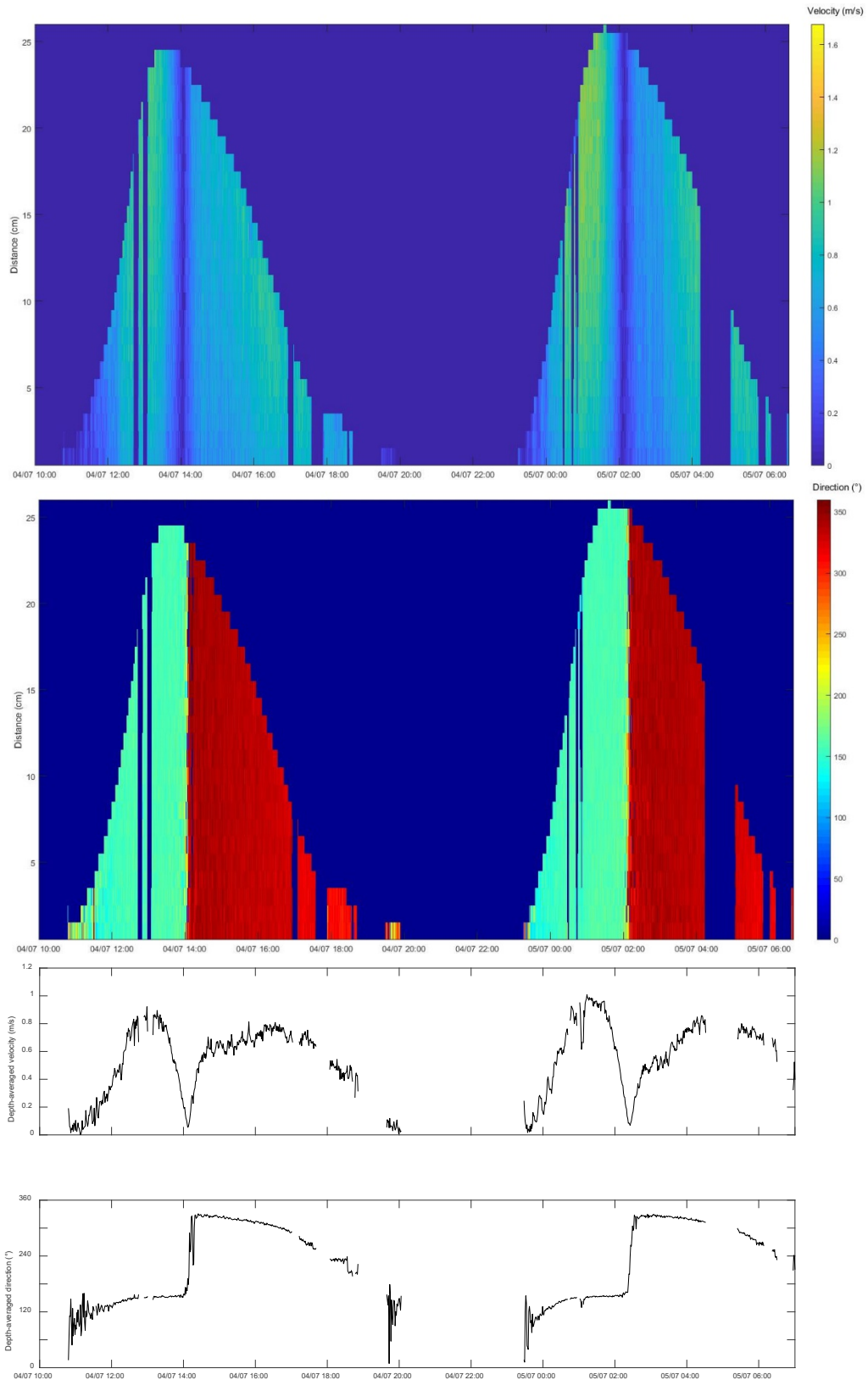


Figure 18 – Time series of current velocity profile, direction profile, and depth-averaged for the Aquadopp A.
 Note: Gaps in the time series are due to missing data. Depth-averaged data at low tide were removed.

Aqd B – embankment of the channel

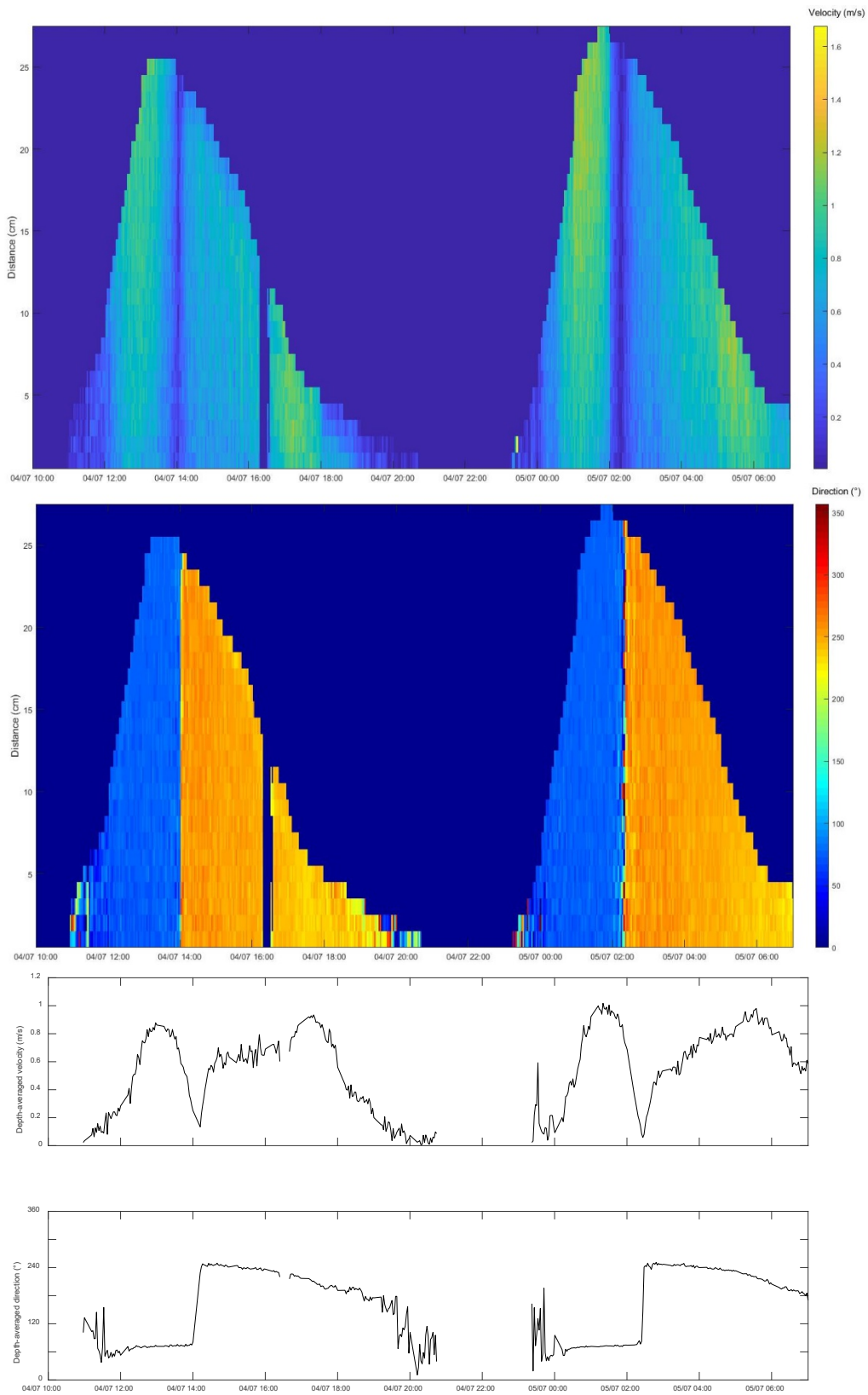


Figure 19 – Time series of current velocity profile, direction profile, and depth-averaged for the Aquadopp B.
 Note: Gaps in the time series are due to missing data. Depth-averaged data at low tide were removed.
 Suspicious current direction records probably caused by the magnetic screws used during the campaign.

Aqd C – in a small puddle at the east side of the channel

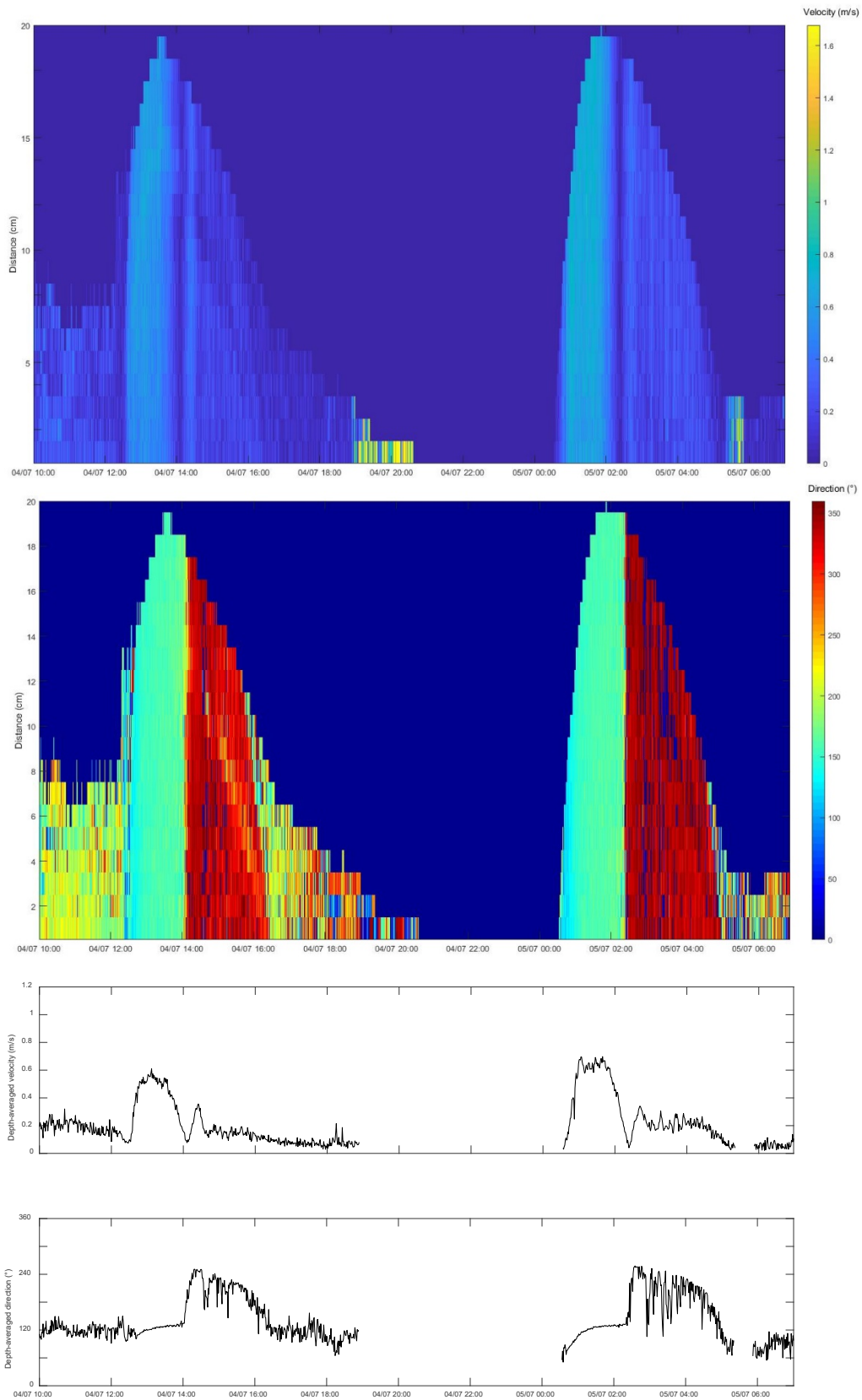
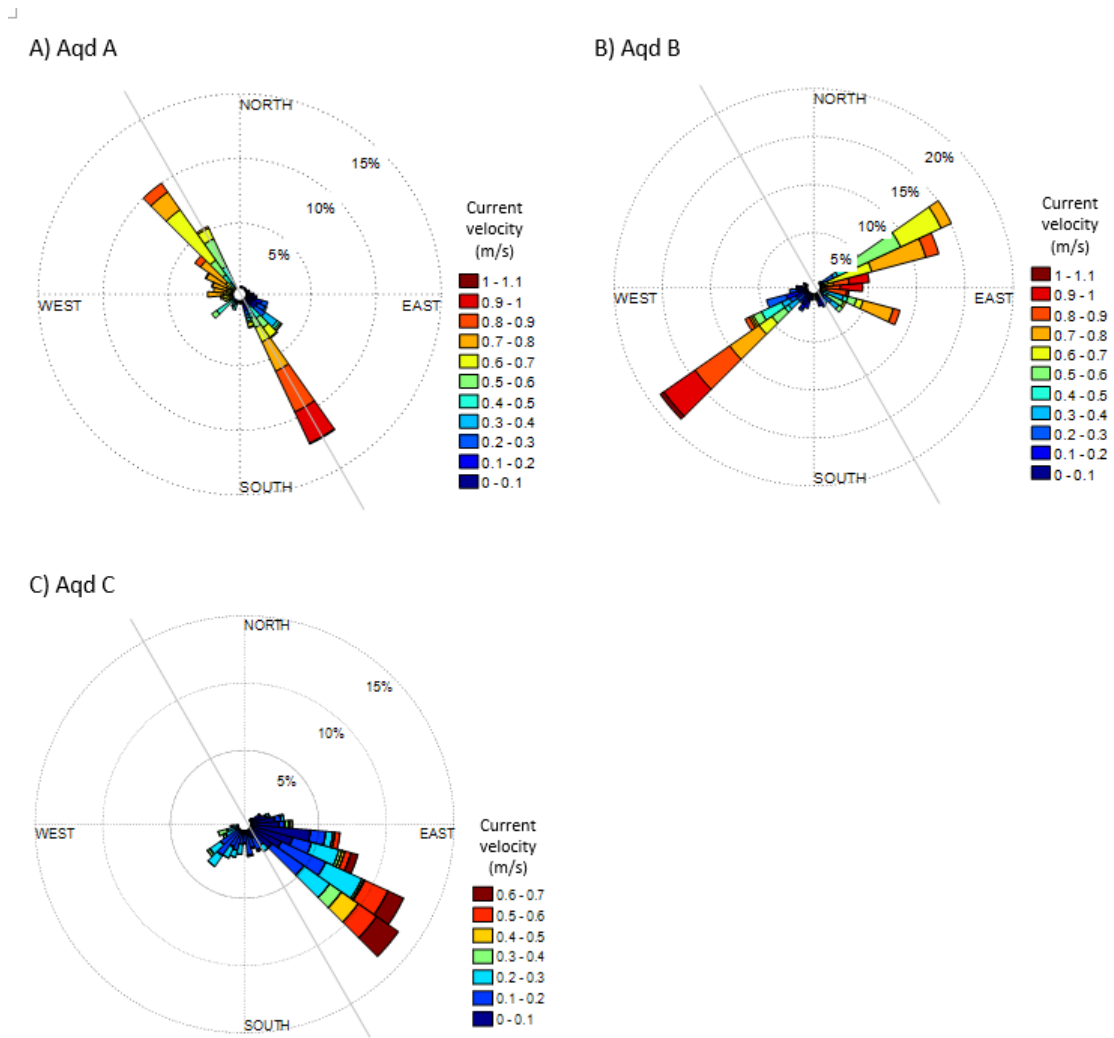


Figure 20 – Time series of current velocity profile, direction profile, and depth-averaged for the Aquadopp C.
 Note: Gaps in the time series are due to missing data. Depth-averaged data at low tide were removed.

Figure 21 presents the current distributions from the three Aquadopps.

Figure 21 – Current distributions from the 3 Aquadopps. Grey line corresponds to the channel orientation (130°-310°). Suspicious current direction records of the Aqd B probably caused by the magnetic screws used during the campaign.



Waves

Wave parameters were recorded by the Aqd B over the entire ad-hoc measurement period (Figure 22). Table 13 summarizes the statistics of the parameters. Waves were characterized by a significant wave height ranging from 0.01 to 0.27 m (average of 0.07 m) with a period of 5 s. They were coming from the N sector in the beginning of the measurements to turn to SW-W from 04/07 at 12:00. The shift of direction on 04/07 from 20:00 to 21:00 and from 23:00 to midnight is more likely due to unreliable records and very low wave height.

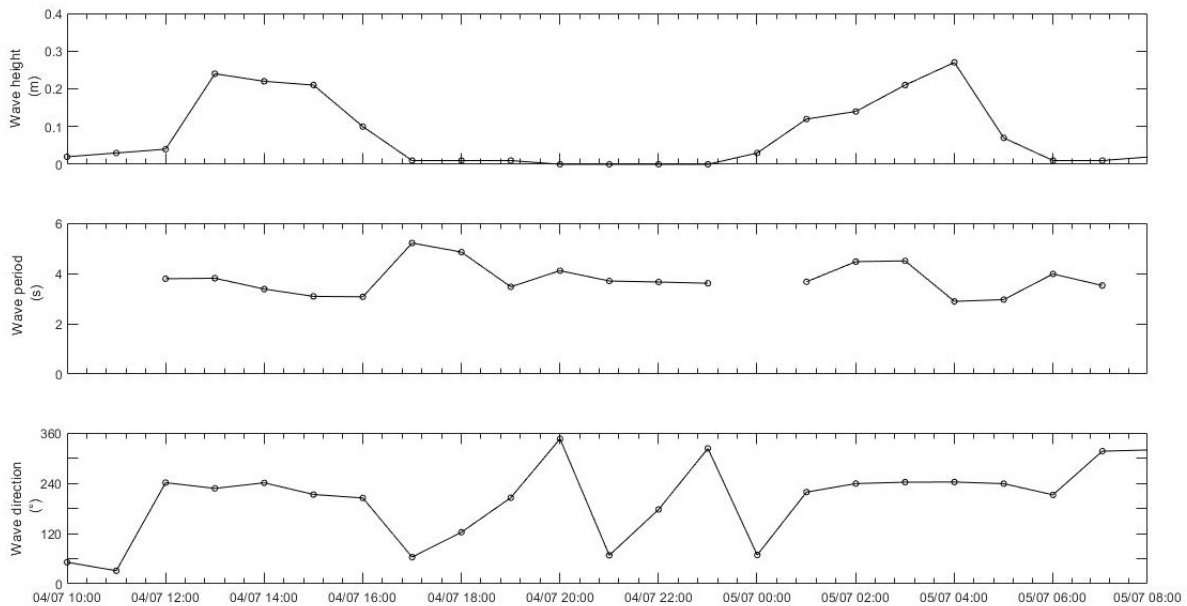


Figure 22 – Time series of significant wave height (H_{m0}), period (T_{m0}) and direction at the Aqd B.

Note: For clarity of the figure, H_{10} and H_{max} are not reported.

The average difference between H_s and H_{10} and H_s and H_{max} is of 0.02 and 0.05 m respectively.

Table 13 – List of the ad-hoc hydrodynamic measurement settings.

Statistics	H_s (m)	H_{10} (m)	H_{max} (m)	T_{m0} (s)	MeanDir (°)
Avg	0.074	0.095	0.123	5.54	194.5
Max	0.27	0.34	0.44	15.06	345.9
Min	0	0	0	2.89	31.24

Cross-channel topography

Figure 23 presents the cross-channel topographic profile acquired on 04/07. It is located up to 60 m seaward from the Aquadopp locations (see Figure 15) so that there is a slight difference between them. The width of the channel is of 100 m with a deepest location around 1.25 m TAW.

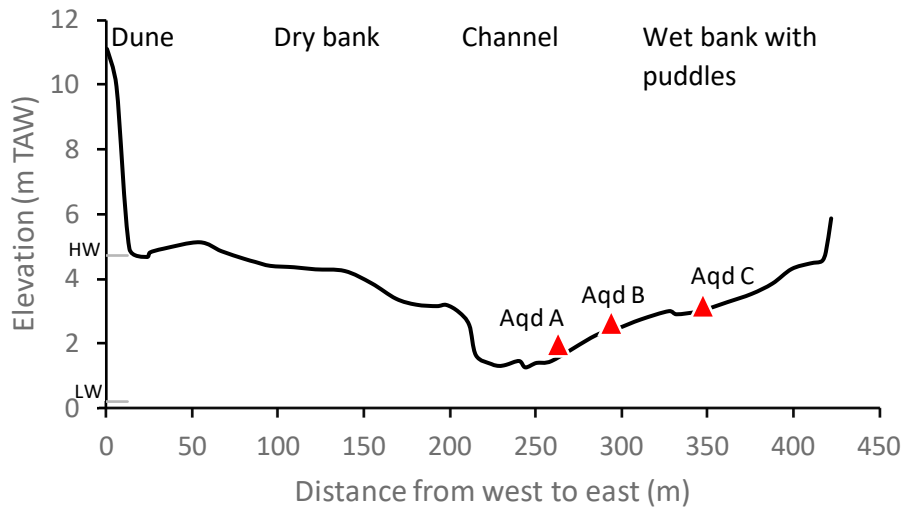


Figure 23 – Cross-channel topographic profile with the Aquadopp locations. Grey lines correspond to the highest water (HW) and low water level (LW) happening during the campaign.

Water discharge

The estimated water discharge across the channel ranged from 20.31 to 323.86 m³/s over the campaign (Figure 24 and Table 14). Our method of estimating water discharge by assuming the current velocity measured by the Aquadopps at a specific location is representative of the velocity for the entire section, in particular near the channel embankments probably overestimate it. However, it gives insight about the pattern of water discharge. As expected, the peak of discharge occurred at high tide when sediments were likely to be flushed into the Zwin (i.e. inflow). The water discharge 1 hour before and after high tide was more than two times lower than at high tide. The water volume flushed in 1 hour before high tide was generally larger than the one flushed out 1 hour after high tide.

The peak value of water discharge is greater than the maximum of 227.51 m³/s occurring just before high tide measured by Aqua Vision for 5 hours on 17/06/2019 characterized by a spring tide and calm condition (Aqua Vision, 2019). This latter campaign was carried out more inside the inlet than the ad-hoc one which might explain the lower values. The Aqua Vision measurements indicated that the water discharge 1 hour before and after high tide was in the same order of magnitude around 100 m³/s.

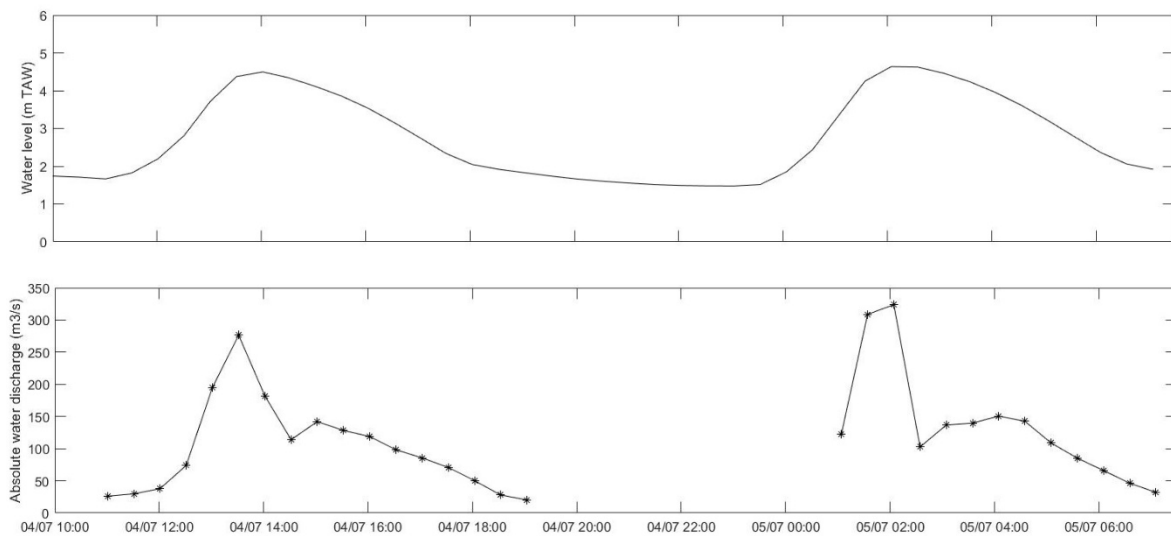


Figure 24 – Time series of 30 minutes averaged water level and estimated water discharge across the channel.

Table 14 – Summary statistics of water discharge across the channel, water level, current velocity and direction measured in the deep channel (Aqd A).

	Water level (m TAW)	Avg. current velocity in the deep channel (m/s)	Avg. current direction in the deep channel (°)	Absolute water discharge (m ³ /s)
3h before 1st HW	1.69	0.07	88.94	25.99
2h before 1st HW	2.01	0.17	120.83	33.78
1h before 1st HW	3.26	0.66	145.99	134.54
HW on 4/7	4.37	0.82	151.97	276.46
1h after 1st HW	4.42	0.40	209.38	147.99
2h after 1st HW	3.99	0.62	323.26	135.16
3h after 1st HW	3.35	0.72	312.60	108.57
1h before 1st HW	3.80	0.84	148.50	215.97
HW on 5/7	4.64	0.84	153.38	323.80
1h after 1st HW	4.54	0.35	253.64	119.67
2h after 1st HW	4.09	0.60	324.11	145.12
3h after 1st HW	3.40	0.76	314.24	125.66

Sediment characteristics

The particle size of the 3 Aquadopp locations is presented in Table 15. The sediment consists of coarse range with a D_{50} from 586 to 639 μm increasing from the deepest channel (Aqd A) to the puddle (Aqd C). The carbonate content is relatively high at the 3 locations (<12%) due to shell fragments.

Table 15 – Statistic summary of the grain size and carbonate content of the three sediment samples collected near the Aquadopps.

Sample	Grain size (μm)							Carbonate content (%)
	d (0.1)	d (0.2)	d(0.350)	d (0.5)	d(0.650)	d (0.8)	d (0.9)	
Aqd A	309.765	377.666	475.116	586.230	729.637	941.840	1179.211	11.73
Aqd B	309.102	382.893	491.901	618.503	780.194	1009.095	1251.377	6.44
Aqd C	292.869	377.595	500.477	639.308	811.622	1051.486	1302.872	10.37

Hydrodynamic processes

The ad-hoc water level records were similar to the Scheur station. There was no delay or alteration of the tide in the Zwin (Figure 25). The current was faster at Scheur station (mean 0.55 m/s with a maximum of 1.26 m/s) than in the Zwin channel. Also, two sudden drops of current velocity occurred 1 hour 10 minutes and 3 hours after high tide at Scheur station, while only one decrease in the Zwin with a short period of 30 minutes. The current at Scheur station was directed to E (90-100°) and WSW (250-270°) during the flood phase and the ebb phase respectively (i.e. from 10° to 20° parallel to the coast). This contrasts with the current in the Zwin channel driven to SSE (150-160°) during the flood and NW (330-340°) during the ebb phase (20-30° from the channel orientation).

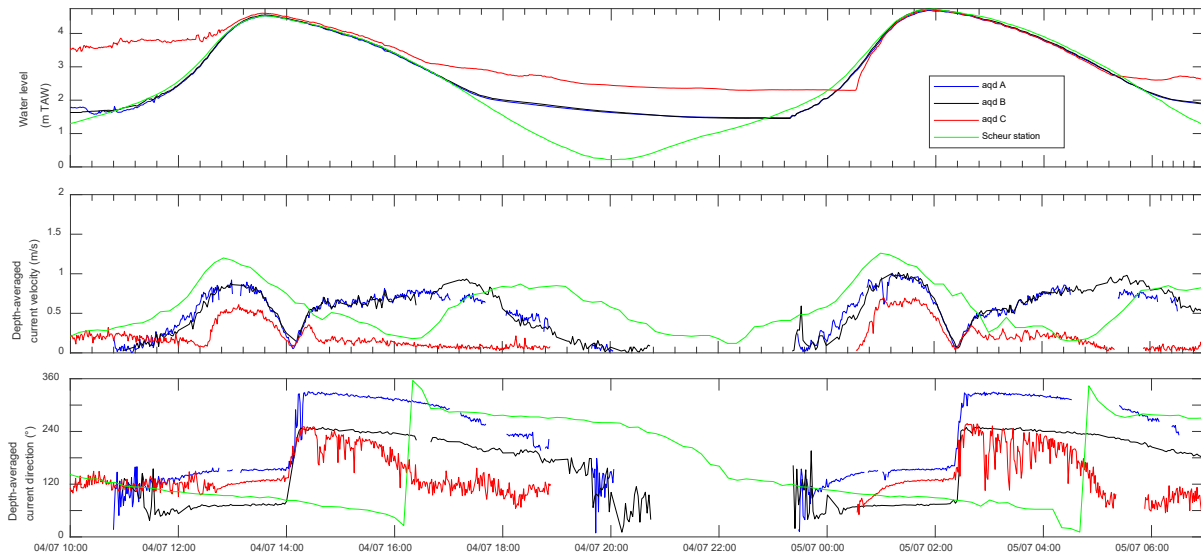


Figure 25 – Time series of water level, depth-averaged of current velocity and direction of the three Aquadopps and Scheur station.

Table 16 presents the average of the depth-averaged current velocity for the three Aquadopps and Scheur station from 1 to 3 hours before or after high tide (HW). In general, the highest current velocity occur one hour before high tide, reaching 0.81 m/s in the deep channel (Aqd A). After high tide, the current velocity progressively increases. Noteworthy, the current velocity 3 hours after tide is equal or slightly higher than at high tide. Regarding the current direction, the shift of flow angle is much higher after high tide than before low tide for all the locations. The flow direction in the Zwin is dictated by the channel orientation while it is the shoreline orientation at the Scheur location. The tidal ellipse is orientated anticlockwise in the North Sea basin (Stroomatlas, 1992).

Table 16 – Statistic summary of the depth-averaged current velocity and direction of the three Aquadopps and Scheur station.

	Depth-averaged current velocity (m/s)				Cell 3	Depth-averaged current direction (°)				Cell 3
	Aqd A	Aqd B	Aqd C	Scheur		Aqd A	Aqd B	Aqd C	Scheur	
3h before 1st HW	0.09	0.10	0.20	0.35	106.79	89.95	118.58	117.00		
2h before 1st HW	0.43	0.36	0.14	0.71	136.45	62.24	118.59	101.50		
1h before 1st HW	0.81	0.80	0.50	1.11	151.41	72.03	120.52	92.50		
HW on 4/7 at 13:35	0.69	0.70	0.53	0.88	151.95	73.18	127.92	91.00		
1h after 1st HW	0.38	0.04	0.25	0.62	223.89	64.66	181.78	79.50		
2h after 1st HW	0.63	0.33	0.15	0.42	322.81	75.25	212.46	63.50		
3h after 1st HW	0.73	0.63	0.12	0.22	311.51	135.90	164.13	4.33		
3h before 1st HW	0.09	0.16		0.75	93.46	95.49		103.40		
2h before 1st HW	0.50	0.40	0.19	1.18	133.69	64.13	79.27	92.67		
1h before 1st HW	0.90	0.92	0.62	0.84	151.01	72.09	119.71	86.43		
HW on 5/7 at 1:50	0.78	0.85	0.58	0.48	153.91	72.66	130.70	70.00		
1h after 1st HW	0.38	0.37	0.28	0.34	230.67	159.95	180.35	72.33		
2h after 1st HW	0.56	0.58	0.21	0.21	324.71	245.31	197.23	86.83		
3h after 1st HW	0.78	0.77	0.20	0.47	317.35	237.49	191.22	9.70		

3.2.5 Summary of the ad-hoc measurement

The first ad-hoc measurement in the Zwin inlet was carried out on 4-5/07/2019 during calm spring condition ($H_s < 0.08$ m coming from SW). The campaign covered approximately 2 tidal cycles (total duration 22 hours) when hydrodynamics were measured at three locations such as in the deep channel, at the east side embankment of the channel and a puddle on the dry beach.

- Current velocity followed the same trend at the three locations with same order of magnitude in the deep channel and embankment, while it was two times lower in the puddle due to its shallow depth.
- Variability of current direction were measured at the three locations which was coherent with tidal phases and the local topography of the sensor deployment. The current in the channel was driven towards SSE ($150-160^\circ$) and NW ($330-340^\circ$) during the flood and ebb phase respectively.
- A common characteristic of the current flow was a sudden drop of velocity and a directional shift 30 minutes after high tide. This also occurred at Scheur station although the decline was lower and more gradual with two drops happening 1 hour 10 minutes and 3 hours after high tide.
- The peak of estimated water discharge was of $323.86 \text{ m}^3/\text{s}$ at high tide. The water discharge one hour before and after high tide was more than two times lower than at high tide (peak). One hour before high tide, the water inflow was generally larger than the outflow one hour after high tide.
- The sediment consists of coarse range (D_{50} around $600 \mu\text{m}$) increasing from the deepest channel to the puddle. The carbonate content is relatively high at the 3 locations ($<12\%$) due to shell fragments.

3.3 Water discharge in the inland inlet

Water discharge in the inland inlet were estimated from the hydrodynamic measurements carried out by Aqua Vision using the remotely-controlled Q-Boat (Appendix A). Figure 26 shows the time series of discharge during the campaign before (23/10/2018, no data available for the campaign in January 2019) and after the opening of the dyke (16/09/2019). The water level conditions (spring tide) were rather similar, allowing to compare the flow debit in the inlet. The maximum flood discharge on 23/10/2018 was $106 \text{ m}^3/\text{s}$, while it was 2.5 times higher after the opening of the dyke ($270 \text{ m}^3/\text{s}$) (Table 17). The difference of water discharge between flood and ebb phases was in average up to $45 \text{ m}^3/\text{s}$ and $74 \text{ m}^3/\text{s}$ higher than before the opening of the dyke. The ebb flow started 15 minutes after high tide on 23/10/2018 when the average of water debit was of $23 \text{ m}^3/\text{s}$ and large variations in the ebb flow rates were observed. On 16/09/2019, the ebb flow started 45 minutes after high tide and rose rapidly to a maximum of $141 \text{ m}^3/\text{s}$ which is an increase of nearly 35% compared to the pre-opening condition. The ebb flow rate gradually augmented with an average of water debit of $97 \text{ m}^3/\text{s}$ on 16/09/2019. During both measurement campaigns, the ebb phase lasted longer than the flood phase which results in a tidal asymmetry with a flow rate during flood larger than the ebb causing the silting up of the inlet. It can be expected that this will mainly occur where the flow is less concentrated and decrease rapidly over short distances. The total water discharge that enters the inland inlet during the flood phase was of $4855 \text{ m}^3/\text{s}$ which was more than 6 times greater than before the opening of the dyke. Appendix A summarizes the hydrodynamic and debit measurements from the Aqua Vision.

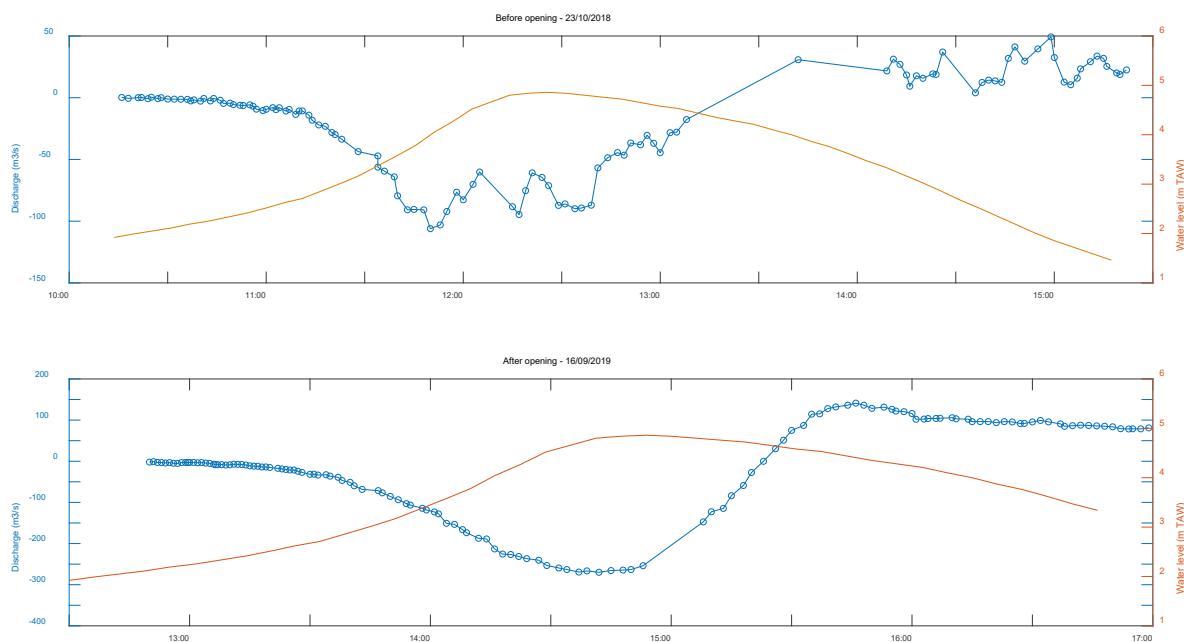


Figure 26 – Measured water level and discharge before (23/10/2018) and after the opening (16/09/2019).

Table 17 – Summary of the debit measurements from Qboat surveys carried out by Aqua Vision.

	Flood discharge (m ³ /s)			Ebb discharge (m ³ /s)		
	Mean	Max	Sum	Mean	Max	Sum
10/07/2017	-32.23	-114.12	-1482.55	17.07	27.85	699.68
18/12/2017	-35.51	-106.24	-2911.88	21.37	40.10	854.62
11/04/2018	-17.82	-54.37	-1907.05	10.25	21.26	778.76
11/07/2018	-27.57	-98.96	-1902.64	15.36	29.14	1305.23
23/10/2018	-37.68	-106.09	-2901.33	23.39	49.25	771.73
01/02/2019	No hydrodynamic measurements					
06/04/2019	-68.11	-175.76	-5176.09	77.20	90.32	2624.94
17/06/2019	-98.87	-227.51	-8700.54	76.78	116.30	5221.13
16/09/2019	-83.12	-269.87	-7397.82	97.10	141.22	4855.11

4 Discussion

4.1 Morphodynamics of the inlet

The results have shown that the Zwin inlet, characterized by a main channel and sandy bedforms of banks and bars, is a dynamic system. After the opening of the dyke on 04/02/2019, significant morphological changes occurred in the entrance channel of the inlet which become nearly 0.5 m deeper and wider up to 18 m. The combination of wave-induced and tidal currents are the main forcing factors driven morphological changes of the inlet entrance. Although there is a high spatial and temporal variability of the mobility of the sandy bedforms, the sediment balance is relatively stable in the entrance inlet unit (period between 06/11/2018-20/04/2019).

The inland inlet unit experiences remarkable morphological changes with an increase of the depth with an average of 0.45 m after the opening of the dyke. Also, the channel becomes wider and migrates toward east. The narrow width of the inland channel is likely to accelerate the velocity of tidal currents which in turn induce erosion. In contrast, the west side of the inland inlet was accreting with the development of sand banks. They were probably supplied by sediment from the entrance inlet. This might explain the relative stability of the sediment budget there versus the material input from the sandy bedforms entering the inlet. This suggests interactions between the entrance and inland inlet units. Bowman (1993) reported that the interactions between topography and tide hydraulics explain the spatial complex of the channel and bedforms in the Zwin as well as their textural trends ranging from coarse sediment grain size and shell deposits in the throat to fine sediment in the inland inlet.

As expected after the expansion of the surface area to over 333 ha, the inlet reacted to the change. Under the increase of the storage area of the inlet, the access channel adjusts by becoming wider and deeper in order to be able to drain larger volumes of water. It is probable that the morphological changes inside the Zwin might be largest just after the intervention work and gradually diminish until it reaches a dynamic equilibrium. Further monitoring is needed to confirm this.

4.2 Tidal Prism

The tidal prism is defined as the amount of water that flows in and out of the tidal inlet during one tidal period. The tidal prism influences the cross-sectional area, the stability of the main inlet channel, as well as controls the intertidal flat area. To estimate the tidal prism, the water basin area is determined, assuming that water levels are uniform within the basin. The tidal prism is derived as (O'Brien, 1969):

$$Tidal\ prism = \int_{Z_{min}}^{Z_{max}} water\ basin\ area\ (z)\ dz$$

where Z_{max} and Z_{min} is the maximum and minimum water level within a tidal period respectively.

In this study, the water basin area was determined using the LiDAR DEMs before (06/11/2018) and after the opening (20/04/2019) covering both the entrance and inland inlet units. The water basin area and volume were determined as a function of water level assuming that water levels are uniform throughout the basin. Since the LiDAR system does not penetrate water, it turns out to be less accurate in the channel. Based on a survey error of 3 cm in vertical, the estimated volume error for a spring water level is below 9770 m³. Figure 27 presents the water basin area, volume as a function of water level (i.e. hypsometry) for the entrance inlet and inland inlet units. As expected, linear relationships are generally found between the area, volume and the water level. Noteworthy, the water basin area of the inland inlet strongly increases between 3 and

3.5 m TAW which might be explained by the flooding of the tidal flats. Also, the results show that the tidal prism that enters in the Zwin is highly dependent on the maximum water level reached during the tidal cycle. Under spring conditions and after the opening of the dyke, the estimations of the water basin volume of the entrance inlet and inland inlet units are 474 625 m³ and 180 350 m³ respectively (based on DEMs). During storm conditions, the combination of surge and high tide is likely to increase the tidal prism for the entire inlet. This needs to be further studied. As previously found, the water basin area and volume of both inlet units after the opening of the dyke have increased up to 1% and 11.2% for the entrance inlet and inland inlet unit respectively. Interestingly, the water basin area of the entrance inlet below 4.7 m TAW after the opening of the dyke was lower than before. However, the water basin volume with a water level ≥ 3 m TAW after the opening is always higher. This confirms again that the water basin has become deeper at the entrance. If the width of the channel continue to enlarge, the tidal prism will also increase. A deepening of the channel in the entrance and inland inlet units with 0.5 m will result to an increase of the tidal prisms of 73 550 m³ and 44 133 m³ respectively. A gradual growth of the tidal prism thus enhances the drainage of the inlet which reduce the silting up process. If the channel keeps increasing its width and depth, the salt marshes might become eroded at some point, but this trend still is to be confirmed by the future topographic measurements.

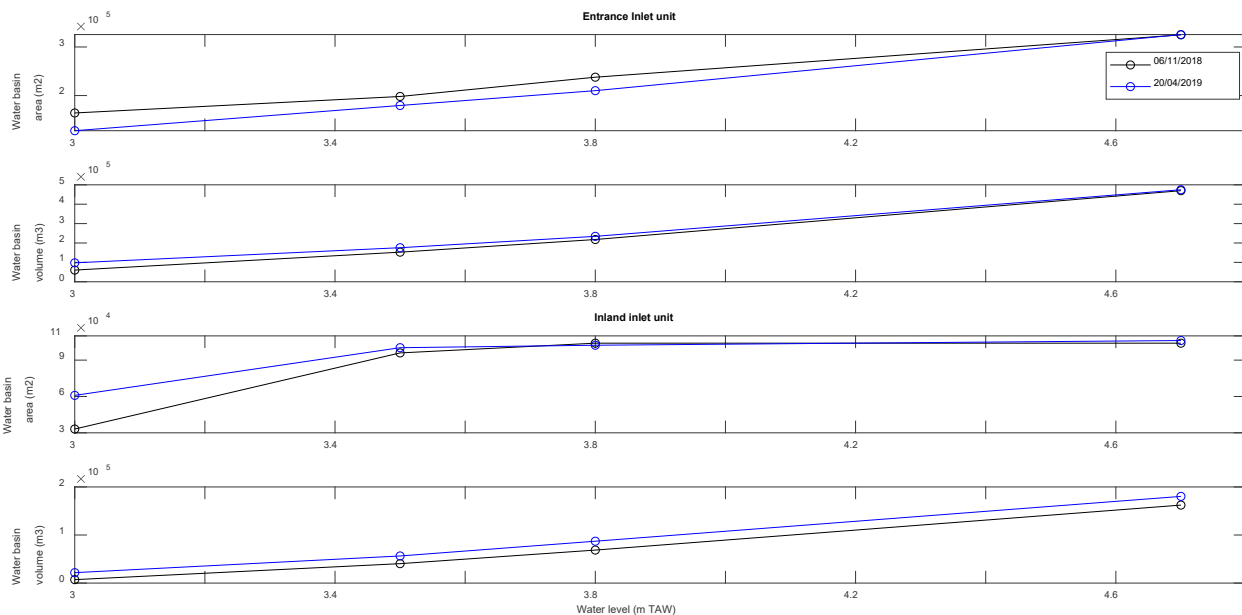


Figure 27 – Hypsometry of the Zwin before (06/11/2018) and after the dyke opening (20/04/2019) as function of water level. Note the difference of y-axes.

The hydraulic measurements in the inland inlet from July 2017 to September 2019 clearly indicate that the water discharge going in and out has strongly increased after the opening of the dyke (> 4000 m³/s after June 2019). Aqua Vision (2019) estimated that the total volume that enters the survey area during the flood phase is 17% larger than in 03/2019. In addition, there is less temporal variability of the water debits following a clear cyclic pattern. The last survey in September 2019 indicates a shift of the start of the ebb flow starting about 45 min after high tide compared to 15 min for the previous measurements. Although it needs to be confirmed this trend would suggest that changes not only occur for the tidal prism and water discharge but also for the tidal duration asymmetry in the inland inlet.

4.3 Forcing factors in the inlet

The presence of the 3D developed sandy bedforms in the seaward side of the entrance of the inlet reflects an ebb-delta organization. Bowman (1993) suggested that the typical ebb delta swash platform bedforms are displaced shoreward in the Zwin. The relatively undeveloped ebb tidal-delta indicates a dominance of onshore sediment transport, which usually occurs in secondary tidal inlet type as here. Ebb tidal deltas have little preservation in stagnating inlets due to their decreases of tidal prism (Oost, 1992). This would suggest that the increase of the tidal prism of the Zwin might favour the occurrence and development of sandy bedforms. Further investigations needs to be done to confirm this hypothesis.

As suggested previously, the maximum water level during the tidal cycle is the major forcing factor of the hydro- and morphodynamics of the Zwin. The study of van der Vegt and Hokstra (2012) on the Slufter in Texel indicates a rapid morphological development of the inlet under energetic hydrodynamic conditions, while it evolves relatively slowly under long period of calm conditions. The authors reports that Slufter is a storm-dominated tidal inlet. The past topographic surveys (LiDAR and Qboat) do not make possible to investigate storm impact of the inlet morphology due to the large time interval between the storm surge event and the survey. Further monitoring will help to improve our understanding on the forcings in the Zwin inlet and how it evolves during energetic conditions, in particular under storm surge event.

5 Conclusions

The tidal inlet is a complex morphological system controlled by waves, tidal range, tidal prism and sediment supply variability. This study reports the morpho- and hydrodynamics of the entire tidal inlet from the pre- to 8 months after opening of the dyke using different types and sources of measurements. The results show that the Zwin inlet is characterized by a main channel and mobile sandy bedforms such as banks and bars, as well as salt marshes and tidal flats. After the opening of the dyke on 04/02/2019, significant morphological changes occur in the channel of the entrance unit, located seaward of the inlet, which becomes nearly 0.5 m deeper and wider up to 18 m. The combination of wave-induced and tidal currents are the main forcing factors driven morphological changes of the entrance inlet. The relative stability of the sediment balance in the entrance contrast with the overall erosion of the inland inlet where the bed elevation decreases of 0.18 m. The inland inlet unit experiences remarkable morphological changes with an increase of the depth with an average of 0.45 m after the opening of the dyke. Also, the channel becomes wider and migrates toward east. However, the west side of the inland inlet is in accretion with the development of sand banks. This probably results in a sediment supply from the entrance inlet suggesting some process interactions between the units.

After the expansion of the surface area to over 333 ha, the inlet changed its morphology. The channel adjusts progressively by becoming wider and deeper in order to be able to drain larger volumes of water estimated to increase of 1% and 11.2% for the entrance and inland inlet unit respectively (period 06/11/2018-20/04/2019). In addition, the difference of water discharge for the flood and ebb phases was in average up to 45 m³/s and 74 m³/s, higher than before the opening of the dyke. The water discharge is characterized by a smooth transition with a clear cyclic pattern between tidal phases after the opening of the dyke. It is probable that the morphological changes inside the Zwin inlet might be the largest after the intervention work and then gradually diminish until it reaches a dynamic equilibrium. Further monitoring is needed to confirm this and to improve our understanding on the forcing factors, processes and responses in the Zwin inlet under energetic conditions (short-term) as well as its long-term evolution.

6 References

- Aqua Vision** (2019) Het Zwin Bathymetrie en stromingsmetingen juni 2019, 25p.
- Bowman, D.** (1993) Morphodynamics of the stagnating Zwin inlet, The Netherlands, *Sedimentary Geology*, 84, 219-239.
- Hartmann, D., Bowman, D.** (1993) Efficiency of the log-hyperbolic distribution – a case study: pattern of sediment sorting in a small tidal-inlet – Het Zwin, The Netherlands. *Journal of Coastal Research*, 9 (4), 1044-1053.
- Houthuys, R., Verwaest, T., Trouw, K.; Mostaert, F.** (2020). Morfologische evolutie van de Vlaamse kust tot 2019. Versie 0.1. WL Rapporten, 18_142. Waterbouwkundig Laboratorium: Antwerpen.
- Cooper, J.A.G.** (2001) Geomorphological variability among microtidal estuaries from the wave-dominated South African coast. *Geomorphology*, 40, 99-122.
- De Swart, H.E., Zimmerman, J.T.F.** (2009). Morphodynamics of tidal inlet systems. *Annual Review of Fluid Mechanics*, 41, 203-229.
- FitzGerald, D., M.** (1996) Geomorphic variability and morphologic and sedimentologic controls on tidal inlets. *Journal of Coastal Research*, 23, 47-71.
- Houthuys, R., Trouw, K., De Maerschalck, B., Verwaest, T., Mostaert, F.** (2013). Inschatting van de morfologische impact van strandsuppleties te Knokke op het Zwin en de Baai van Heist. Versie 4.0. WL Rapporten, 12_107. Waterbouwkundig Laboratorium & IMDC: Antwerpen, België.
- Lincoln, J.M., FitzGerald, D.M.** (1988) Tidal distortions and flood dominance at five small tidal inlets in southern Maine. *Marine Geology*, 82, 133-148.
- O'Brien, M.P.** (1969) Equilibrium flow areas of inlets on sandy coasts. *Journal of Waterway Port Coast Ocean Engineering* 95 (1) 43-52.
- Oost, A.P.** (1992) Sedimentological implications of the closure of the Lauwersea and the developmebnt of the Frisian inlet system. 3rd International Research Symposium of Modern and Ancient Clastic Tidal Depositis, Wilhelmshaven, 107.
- Stroomatlas** (1992) Noordzee Vlaamse Banken, Dienst der kusthavens hydrograpjie Oostende, 29p.
- Temmerman, S., Meire, P., Bouma, T.J., Herman, P.M.J., Ysebaert, T., De Vriend, H.J.** (2013) Ecosystem-based coastal defence in the face of global change, *Perspective*, 504, 79-83.
- Trouw, K., Zimmermann, N., Li, W., De Maerschalck, B., Delgado, R., Verwaest, T., Mostaert, F.,** 2015. Scientific support regarding hydrodynamics and sand transport in the coastal zone, Literature and data review coastal zone Zeebrugge – Zwin. Version 4_0. WL Rapporten 12_107. Flanders Hydraulics Research. Antwerp, Belgium, 74p.
- Van Bohemen, H.D.** (1996) Environmentally friendly coasts: dune breaches and tidal inlets in the foredunes. *Environmental engineering and coastal management. A case study from the Netherlands. Landscape and Urban Planning*, 34, 197-2313.

Van der Vegt, M., Hoekstra, P. (2012) Morphodynamics of a storm-dominated, shallow tidal inlets: the Slufter, the Netherlands. *Netherlands Journal of Geosciences*, 991-3, 325-339.

ZTAR Newsletter (2017) Het Zwin revived! Zwin tidal area restoration. 1-16.

Appendix A

Aqua Vision data acquisition and results extracted from reports

A.1. Inleiding

Het Zwin is een getijdenlandschap gelegen op de grens tussen Nederland en België (zie Figuur 1). Het gebied staat nagenoeg droog met laagtij en overstroomt naar mate het hoogtij wordt, in het bijzonder in combinatie met stormopzet. In opdracht van IVA MDK, Afdeling Kust (hierna te vernoemen: AMDK) heeft Aqua Vision BV (hierna te vernoemen: AV) bathymetrie- en stromingsmetingen uitgevoerd in natuureservaat het Zwin.

Data is verkregen met behulp van de radiografisch bestuurbare *Q-boat 1800RP* van *Teledyne Instruments RD*, waarin een *Acoustic Doppler Current Profiler (ADCP)* en een RTK-GPS systeem zijn geïnstalleerd. Met dit meetstelsel kan de hoogteligging van de waterbodem bepaald worden, alsmede de stroomsnelheden worden gemeten. Uit deze combinatie van meetdata kan het debiet worden berekend.



Figuur A.1. Overzicht van Het Zwin gebied. Foto van vóór de doorbraak (8 mei 2018, bron Google Earth).

A.2. Meetmethoden

Voor de metingen zijn een ADCP en een RTK-GPS systeem gebruikt. Deze systemen zijn geïnstalleerd op de radiografisch bestuurbare surveyboot (Q-boat) van AMDK. Hiermee zijn meettraaien door het gebied gevaren.

A.2.1 ADCP

De profielmetingen zijn uitgevoerd met een *Acoustic Doppler Current Profiler (ADCP)* van het merk Teledyne RD Instruments (zie Figuur 2), type RiverPro. Dit meetinstrument heeft 5 bundels. Eén verticale bundel en 4 bundels onder een hoek van 20 graden in een Janus configuratie.

De verticale bundel heeft een zendfrequentie van 600 kHz; de vier gekantelde bundels een frequentie 1200 kHz. Iedere bundel zendt twee type pulsen uit: korte en lange pulsen. Korte pulsen worden gereflecteerd door deeltjes in het water en door de beweging van de deeltjes ten opzichte van de ADCP ontstaat er een frequentieverandering (Doppler shift). Deze frequentieverandering gebruikt het instrument voor het berekenen van de watersnelheid en –richting. Lange pulsen worden gebruikt voor het meten van de verplaatsing van het instrument ten opzichte van de bodem (*bottom-track*). De *bottom-track* wordt

gebruikt om de waterdiepte onder de ADCP te bepalen en op deze wijze wordt de bodemligging onder water (bathymetrie) in kaart gebracht.

Door raaien te varen dwars op de stroomrichting wordt met de *bottom-track* het doorstroomoppervlak bepaald, welke in combinatie met de stroomsnelheid het debiet oplevert.



Figuur A.2. De gebruikte ADCP van Teledyne RD Instruments, RiverPro.

De instellingen van de ADCP tijdens de metingen zijn weergegeven in Tabel 1.

Tabel A.1. ADCP meetinstellingen.

HARDWARE	
ADCP type	TRDI RiverPro
Serienummer	1155
Firmware-versie	56.03
Bundelhoek	20 graden
Frequentie	1200 kHz
Aantal bundels	5 (waarvan 1 verticale, 600 kHz)
ADCP oriëntatie	Neerwaarts
Bundeloriëntatie	Convex
MEETINSTELLINGEN	
Maximale diepte	25 m
Aantal pings per ensemble voor watercellen	1
Aantal pings per ensemble voor bodem	1
Ensemble interval	2 per seconde
Celgrootte (hoogte)	Variabel (door instrument bepaald)
CALIBRATIE GEGEVENS	
ADCP insteekdiepte	10 cm
Geluidssnelheid	berekend uit temperatuurgegevens
<i>Pitch & roll</i> compensatie toepassen	Ja

A.2.2 RTK-GPS

Een extern GPS-systeem is gebruikt voor het vastleggen van alle metingen in een geografisch coördinatenstelsel (welke omgerekend zijn naar UTM 31N en TAW). Hiervoor is gebruikgemaakt van een RTK-GPS ontvanger van het merk Septentrio (type: AsteRx2deH).

Deze GPS is uitgerust met een GSM-modem en een SIM-kaart. Hiermee werd verbinding gemaakt met het internet en contact gelegd met het RTK 06GPS netwerk. Op basis van de positie van de GPS-antenne wordt een virtueel referentiestation aangemaakt vlak bij de meetlocatie. Dit levert GPS-correcties op die *real-time* worden verzonden via het internet naar de GPS-antenne op de meetlocatie. Hiermee wordt de GPS met een zogenaamde RTK-Fix uitgevoerd en wordt er een nauwkeurigheid bereikt in de plaatsbepaling van op zijn minst 2 centimeter in het horizontale vlak en 3 centimeter in het verticale vlak.

De ADCP is uitgerust met 5 geluidsbundels. Dit betekent dat per meting op 5 locaties de bodemdiepte wordt bepaald. De enkele verticale bundel, de 4 bundels met bundelhoek van 20 graden, het interne kompas, *pitch- & roll* sensor, de GPS en de lokale waterdiepte bepalen uiteindelijk de locatie van de dieptemeting.

A.2.3 Survey boot

Voor het in kaart brengen van de bathymetrie en het meten van de debieten is de radiografisch bestuurbare *Q-boat 1800RP* van *Teledyne RD Instruments* gebruikt (zie Figuur 3). De Q-Boat bevat twee buitenboordmotoren (die een topsnelheid van 5 m/s mogelijk maken), gecombineerd met de optimale uitlijning maakt dit het mogelijk de boot in te zetten bij hoge stroomsnelheden.

De ADCP en de GPS zijn via draadloze communicatie (radiomodems) verbonden aan een laptop bij de surveyor op de oever. Het meetsysteem wordt gevoed door een accu in het meetvaartuig. Met behulp van *ViSea Data Acquisition Software (DAS)* en bijbehorende *Survey Toolbox (STB)*, is de ADCP aangestuurd en zijn alle data simultaan ingewonnen en opgeslagen.



Figuur A.3: De AMDK Q-boat 1800RP van Teledyne RD Instruments.

A.3. Validatie en verwerking

Bij de verwerking van de data zijn alle instellingen gecontroleerd, waar nodig aangepast en vervolgens zijn alle gegevens opnieuw berekend en uitgevoerd. De verwerking van de bathymetrie en stromingsmetingen zijn uitgevoerd met ViSea. Alle gegevens zijn gecontroleerd op fouten als uitschieters in de *bottom-track* data. Voor alle metingen geldt dat RTK-Fix beschikbaar was.

A.3.1 Bathymetrie

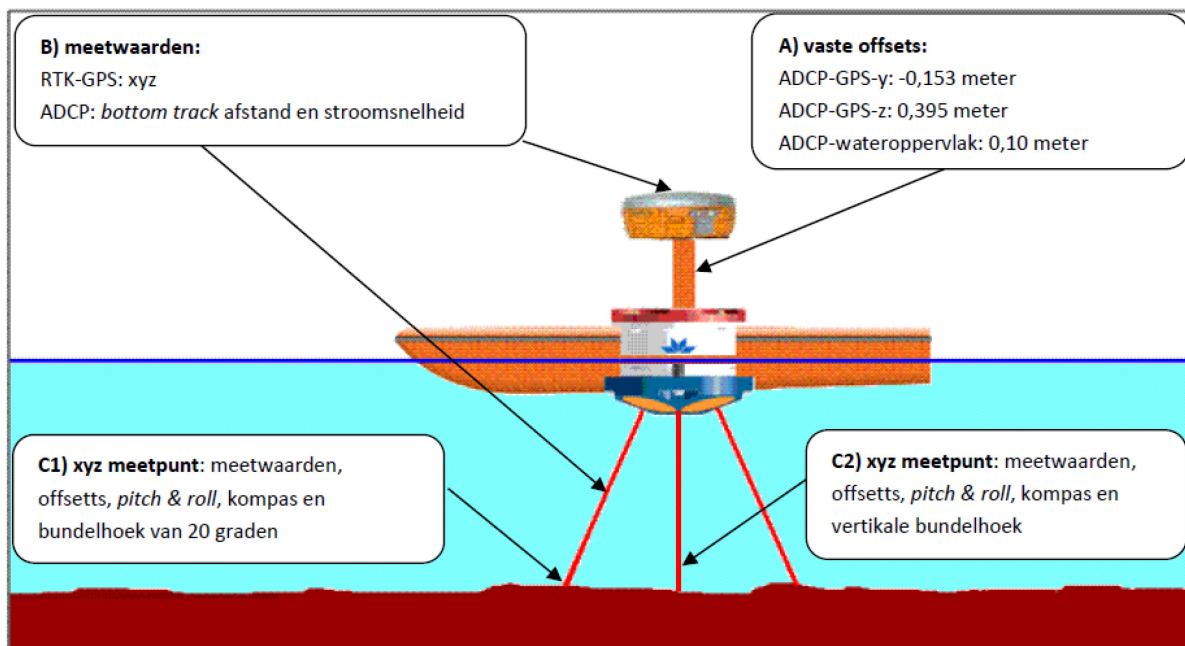
De methodiek van verwerking is als volgt:

A) De afstanden (*offsets*) tussen de GPS, het waterniveau en de *transducer* van de ADCP zijn bekend (zie Figuur 5);

B) De GPS meet de ligging in het XYZ-vlak en de *bottom-track* van de ADCP meet per bundel met een frequentie van 4-6 Hz de diepte ten opzichte van de *transducerhead*. De ADCP-metingen worden automatisch voor *pitch & roll* gecorrigeerd

C) De ingewonnen data worden op kantoor verwerkt en gevalideerd (ViSea Data Presentation Software en Autoclean) zodat de ligging van de waterbodem bepaald wordt in UTM zone 31 N coördinaten en ten opzichte van TAW (z-waarde);

D) De bathymetrie data wordt vervolgens geïnterpoleerd (*Qinsy*) tot een raster met cellen van 20 cm.



Figuur A.4. Meetopstelling voor bathymetrische metingen.

A.3.2 Stroomsnelheid

Validatie van de gemeten stroomsnelheid omvat het per track controleren op foutieve meetwaarden zoals uitschieters. Alle ADCP metingen zijn in ViSea DPS gevalideerd waarbij de data op basis van verschillende criteria (zoals *error velocity*, *correlation magnitude* en *percent good*) zijn getoetst. Foutieve waarden (uitschieters) zijn verwijderd en geïnterpoleerd ten behoeve van de debietberekeningen. De stromingsdata zijn niet geëxtrapoleerd tot de oevers.

A.4. Resultaat

A.4.1. Stroming en debiet

Survey	Result	Figure: Water level and water debit
10,11/07/2017	<p>Om een eerste indruk te krijgen van de (getij)stroming in het gebied zijn er dwarsraaien gevaren. Deze meetraai verplaatste met de bathymetrische metingen mee van noord naar zuid. De gemeten stromingsdata op 10 en 11 juli wordt gepresenteerd in Bijlage 1.</p> <p>Uit de gemeten stroomsnelheidsdata zijn debieten berekend met behulp van ViSea. De debieten gemeten op 10 juli 2017 zijn het meest betrouwbaar aangezien de metingen in het smalste en meest toegankelijke deel van het gebied zijn genomen; in meest noordelijke deel van het bemeten gebied, daar waar het strand overgaat in het achterliggende natuurgebied. Verder weg van deze locatie kan er pas later worden begonnen met meten (hogere ligging) en worden de raaien langer. In sommige gevallen zijn kleine geulen niet bemeten worden als de voorliggende zandbank te ondiep was.</p> <p>Vloedstroom: Uit de figuren kan worden opgemaakt dat bij opkomend tij er water het Zwin instroomt vanaf een waterhoogte van ongeveer +3 m TAW. Vanaf dit moment stijgt het debiet zeer snel tot een maximum van circa 100 m³/s. Het verschil tussen de pieken van beide dagen wordt verklaard doordat op 11 juli meer landinwaarts, voorbij een belangrijke zijtak, is gemeten.</p> <p>Na de maximale vloedpiek daalt het debiet tot ongeveer 25 m³/s, waarna er weer een (kleine) stijging wordt waargenomen van 5 m³/s. Opmerkelijk is dat deze korte piek zichtbaar is op beide dagen. Deze kleinere piek in de vloed wordt zeer waarschijnlijk veroorzaakt door het overstijgen van een zandbank, waardoor er extra toevoer ontstaat.</p> <p>Ebstroom: De duur van de ebstroom is beduidend langer en minder sterk dan de vloedstroom. Dit proces heet getijasymmetrie en is een van de oorzaken van verzanding van het gebied. Vanaf een kwartier na hoog water begint de ebstroom. Het water stroomt het gebied uit met sterk variërende debieten; maximaal 25 m³/s De langere ebduur en de variaties in de ebstroom debieten worden verklaard door verschillen in de wrijvingsfactoren, zoals ondieptes en vegetatie. Op 11 juli is er een dalende trend zichtbaar aan het einde van de meting, waarbij het debiet richting 0 m³/s gaat. De kentering ontstaat hier wederom vanaf circa +3 m TAW.</p>	<p>Figure: Water level and water debit</p> <p>Figuur 9: Getij en gemeten debiet op 10 juli 2017. Negatief debiet duidt op vloedstroom, positief debiet duidt op ebstroom.</p> <p>Figuur 10: Getij en gemeten debiet op 11 juli 2017. Negatief debiet duidt op vloedstroom, positief debiet duidt op ebstroom.</p>

<p>18,19/12/ 2017</p>	<p>Om ook debieten te kunnen bepalen, die door het getij door de hoofdgeul stromen, zijn de bathymetrische meetraaien telkens dwars op de stroming gevaren. Het gebied is ingemeten vanuit de zeezijde landinwaarts. De gemeten stromingsdata op 18 december wordt gepresenteerd in Bijlage 1. Uit de gemeten stroomsnelheidsdata zijn debieten berekend met behulp van ViSea. De debieten gemeten op 18 december 2017 zijn het meest compleet aangezien de metingen in het smalste en meest toegankelijke deel van het gebied zijn genomen; in het meest noordelijke deel van het bemeeten gebied. Verder landinwaarts kan er pas later worden begonnen met meten (hogere ligging) worden de meetraaien langer. In sommige gevallen zijn kleine geulen niet bemeeten, bijvoorbeeld als de voorliggende zandbank te ondiep was. Vloedstroom: Vanaf dit moment stijgt het debiet zeer snel tot een maximum van circa 100 m³/s. Na de maximale vloedpiek daalt het debiet tot ongeveer 37 m³/s in december (t.o.v. 25 m³ in juli), waarna er weer een stijging wordt waargenomen circa 10 m³/s (t.o.v. 5 m³/s in juli). Wellicht is de zandbank die overstegen wordt (Aqua Vision 08/2017), waardoor deze piek vermoedelijk ontstaat, hoger geworden. Hierdoor verschijnt deze piek later (+ 4,5 m TAW in december) en is de extra water toevoer hoger. Het totale volume water wat met de vloedstroom binnenkwam is berekend op 30.9780 m³ versus 25.4960m³ voor respectievelijk december en juli 2017. Dit is een verschil van circa 20%). Het hogere totale volume gemeten in december zal grotendeels verklaard worden door de circa 15 cm hogere waterstand. Maar dit kan ook het gevolg zijn van de uitbreidingen van het getijddebekken, door de huidige werkzaamheden in het gebied.</p> <p>Ebstream: Evenals in juli begint in december een kwartier na hoog water de ebstream. Het water stroomt nog steeds het gebied uit met sterk variërende debieten; maximaal 25 m³/s. De variaties in de ebstream debieten worden verklaard door verschillen in de wrijvingsfactoren, zoals ondieptes en vegetatie.</p> <p>Getij asymmetrie: Voor beide campagnes (juli versus dec 2017) geldt dat de ebfase langer duurt dan de vloedfase. Dit wordt getijasymmetrie genoemd, waarbij hoge vloodsnelheden t.o.v. ebsnelheden (op de lange termijn!) zorgen voor verzanding (Eng: <i>tidal pumping</i>). De gemeten duur van de vloedperiode is in de laatste campagne (dec 2017) toegenomen waardoor het effect van getijasymmetrie in principe wat zal afnemen. Het betreft hier echter een enkele meting. Hoe het Zwin landschap uiteindelijk zal reageren op de werkzaamheden wordt pas zichtbaar over langere tijd.</p>	<p>Figuur 14: Getij en gemeten debiet op 18 december 2017. Negatief debiet duidt op vloedstroom, positief debiet duidt op ebstream.</p> <p>Figuur 15: Getij en gemeten debiet op 10 juli 2017. Negatief debiet duidt op vloedstroom, positief debiet duidt op ebstream.</p>
-----------------------	--	---

12,13/04/2018

Om debieten te bepalen door de hoofdgeul, zijn de bathymetrische meetraaien telkens dwars op de stroming gevaren. Het gebied is ingemeten vanuit de zeezijde, landinwaarts. De gemeten stromingsdata worden weergegeven in presentaties, welke zijn meegeleverd met deze rapportage.

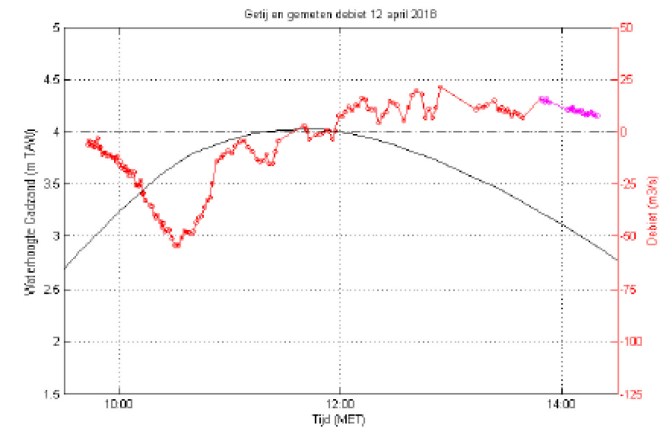
Uit de gemeten stroomsnelheidsdata zijn debieten berekend met behulp van ViSea. De debieten gemeten op 12 april 2018 zijn het meest compleet aangezien de metingen in het smalste en meest toegankelijke deel van het gebied zijn genomen; in het meest noordelijke deel van het bemeeten gebied. Verder landinwaarts kan er pas later worden begonnen met meten (hogere ligging) worden de meetraaien langer. In sommige gevallen zijn kleine geulen niet bemeeten, bijvoorbeeld als de voorliggende zandbank te ondiep was.

Vloedstroom: Zichtbare verschillen in afvoer worden verklaard door de circa 70 cm lagere maximale waterstand in april vergeleken met de metingen in december. Dit verschil van 70cm wordt verklaard door een kleinere getijslag. Dit is ook zichtbaar in de getijvolumes. Het totale volume water wat met de vloedstroom binnen stroomde, is berekend op 159.850 m³ (april 2018). Gedurende de metingen in december 2017 was dit 309.780 m³.

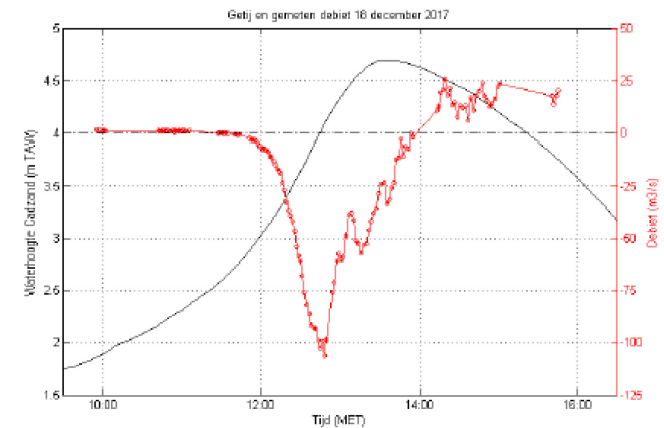
Uit een verdere vergelijking tussen Figuren kan worden opgemaakt dat de waterhoogte waarbij er met opkomend tij water het Zwin instroomt nog steeds onveranderd is (ca. + 3 m TAW, Aqua Vision 12/2017). Vanaf dit moment stijgt het debiet tot een maximum van 55 m³/s.

Ebstroom: Evenals de vorige meetcampagnes begint een kwartier na hoog water de ebstroom. Het water stroomt het gebied uit met sterk variërende debieten; maximaal ca. 20 m³/s. De variaties in de ebstroom debieten worden verklaard door verschillen in de wrijvingsfactoren, zoals ondieptes en vegetatie.

Getij asymmetrie: Voor de campagne in april 2018 geldt wederom dat de ebfase langer duurt dan de vloedfase (evenals in juli en december 2017). Dit wordt getijasymmetrie genoemd, waarbij hoge vloodsnelheden t.o.v. ebsnelheden (op de lange termijn!) zorgen voor verzanding. Vanwege de kleinere amplitude van de getijkromme kan de duur van de vloedstroom in april 2018 niet worden vergeleken met de duur van de vloedstroom in 2017. Omdat het primaire doel van de meting niet is om de gehele getijkromme te bemeeten (zoals bij een 13-uurs meting) is het niet precies bekend hoe lang de ebstroom doorgaat en kan er dus nog geen relatieve duur van de vloedstroom worden berekend.



Figuur 10: Getij en gemeten debiet op 12 april 2018. Negatief debiet duidt op vloedstroom, positief debiet duidt op ebstroom. Het paars debiet gemeten bij de ingang, noordzijde, van het gebied – niet aansluitend in de tijdreeks.



Figuur 11: Getij en gemeten debiet op 18 december 2017. Negatief debiet duidt op vloedstroom, positief debiet duidt op ebstroom.

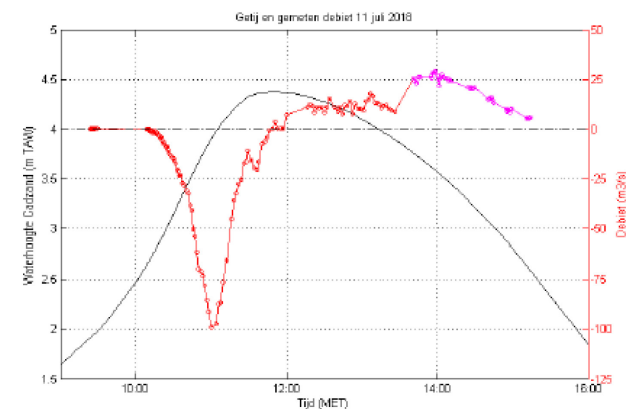
10,16/07/ 2018

Om debieten te bepalen door de hoofdgeul, zijn de bathymetrische meetraaien telkens dwars op de stroming gevaren. Het gebied is ingemeten vanuit de zeezijde, landinwaarts. De gemeten stromingsdata worden gefilterd (zodat het stroombeeld beter zichtbaar is) weergegeven in presentaties, welke zijn meegeleverd met deze rapportage. Uit de gemeten stroomsnelheidsdata zijn debieten berekend met behulp van ViSea. De debieten gemeten op 11 juli 2018 zijn het meest compleet aangezien de metingen in het smalste en meest toegankelijke deel van het gebied zijn genomen; in het meest noordelijke deel van het bemeeten gebied. Verder landinwaarts kan er pas later worden begonnen met meten (hogere ligging) en worden de meetraaien langer. In sommige gevallen zijn kleine geulen niet bemeeten, bijvoorbeeld als de voorliggende zandbank te ondiep was.

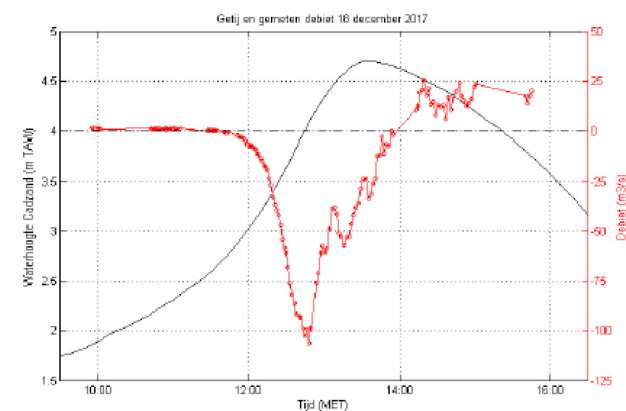
Vloedstroom: De hoogtes van de afvoer zijn zeer vergelijkbaar tussen de twee meetcampagnes met een maximum van rond de 100 m³/s. Bij een waterhoogte van ongeveer 4,3 m TAW begint de afvoer gedurende beide meetcampagnes weer te stijgen, na de piek al eerder gehad te hebben. Deze stijging houdt minder lang aan in de huidige campagne, aangezien de maximale waterhoogte op dit moment bereikt wordt. Het totale volume water wat met de vloedstroom binnen stroomde is berekend op 208.292 m³ (juli 2018). Gedurende de metingen in december 2017 was dit 309.780 m³. Uit een verdere vergelijking tussen

Ebstroom: Evenals de vorige meetcampagnes begint een kwartier na hoog water de ebstroom. Het water stroomt het gebied uit met debieten van rond de 12 m³/s. Wanneer de waterdiepte niet meer voldoende was halverwege het gebied, zijn er debietsmetingen verricht aan de ingang (noordzijde) van het gebied. De variaties in de ebstroom debieten, zoals gezien in eerdere campagnes zijn in de huidige campagne minder tot niet zichtbaar. Wanneer er bij de ingang van het gebied wordt gemeten in deze variatie zo goed als verdwenen en wordt er een geleidelijk afnemende afvoer gemeten.

Getij asymmetrie: Voor de campagne in juli 2018 geldt wederom dat de ebfase langer duurt dan de vloedfase. Dit wordt getijasymmetrie genoemd, waarbij de hoge vloedsnelheden t.o.v. ebsnelheden (op de lange termijn) zorgen voor verzanding. Voor de eerste maal is nagenoeg de gehele vloed- en ebstroom bemeeten (zoals bij een 13-uurs meting). De ebstroom duurde op 11 juli 2018 met 3:30 uur tweemaal langer dan de vloedstroom, welke dus 1:45 duurde.



Figuur 9: Getij en gemeten debiet op 11 juli 2018. Negatief debiet duidt op vloedstroom, positief debiet duidt op ebstroom. In het paars debieten gemeten bij de ingang, noordzijde, van het gebied – niet aansluitend in de tijdreeks.



Figuur 10: Getij en gemeten debiet op 18 december 2017. Negatief debiet duidt op vloedstroom, positief debiet duidt op ebstroom.

23,24/10/2018

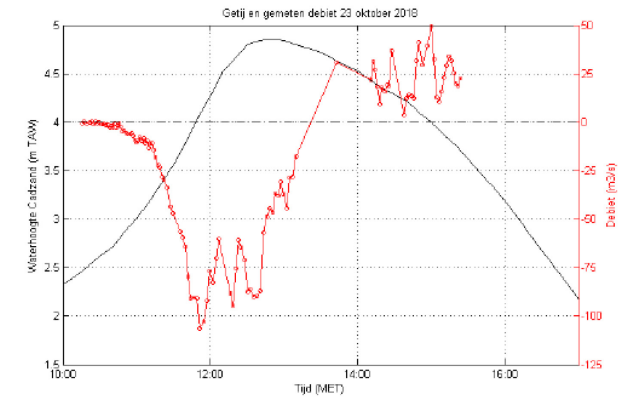
Om debieten te bepalen door de hoofdgeul, zijn de bathymetrische meetraaien telkens dwars op de stroming gevaren. Het gebied is ingemeten vanuit de zeezijde, landinwaarts. De gemeten stromingsdata worden gefilterd (zodat het stroombeeld beter zichtbaar is) weergegeven in presentaties, welke zijn meegeleverd met deze rapportage. Uit de gemeten stroomsnelheidsdata zijn debieten berekend met behulp van ViSea. De debieten gemeten op 23 oktober 2018 zijn het meest compleet aangezien de metingen in het smalste en meest toegankelijke deel van het gebied zijn genomen; in het meest noordelijke deel van het bemeeten gebied. Verder landinwaarts kan er pas later worden begonnen met meten (hogere ligging) en worden de meetraaien langer. In sommige gevallen zijn kleine geulen niet bemeeten, bijvoorbeeld als de voorliggende zandbank te ondiep was. Vanwege de erg hoge waterstand zijn er tussen 13:15 en 13:45 geen dwarsraaien gevaren en dus geen debieten beschikbaar. Figuur geeft het getij en gemeten debiet weer op 23 oktober. Hierin valt op dat het debiet gedurende de vloed van 23 oktober een stuk grilliger verloopt dan op 11 juli. Op basis van deze constatering is de meetdata van 23 oktober andermaal grondig bekeken. Daarnaast is de kwaliteit van de meetdata ook vergeleken met de meetdata van 11 juli. Er zijn geen afwijkingen gevonden in de meetdata die deze “grilligheid” verklaard.

Vloedstroom: De hoogtes van de afvoer zijn zeer vergelijkbaar tussen de twee meetcampagnes met een maximum van rond de $100 \text{ m}^3/\text{s}$, terwijl vanwege de stormopzet de maximum waterhoogte op 23 oktober een halve meter hoger was en hier dus een hoger maximum debiet verwacht wordt. Het lijkt gezien de schommelingen in de piek van de vloedstroom dat hier een deel van het debiet niet bemeeten is.

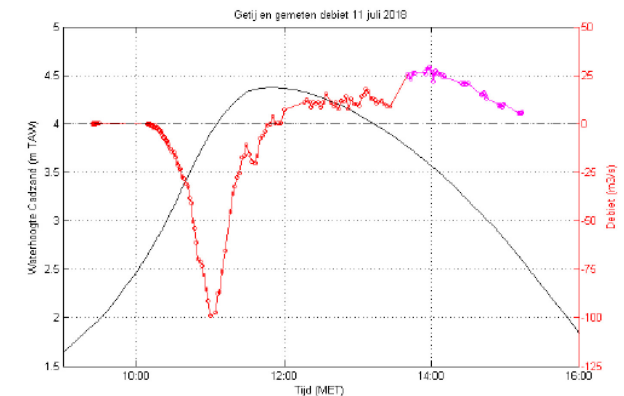
Het totale volume water wat met de vloedstroom binnen stroomde is berekend op 464.731 m^3 (wat vermoedelijk nog hoger is vanwege de gemiste maximale debieten). Gedurende de metingen in juli 2018 was dit 208.292 m^3 . Uit een verdere vergelijking tussen Figuren 11 kan worden opgemaakt dat de waterhoogte waarbij er met opkomend tij water het Zwin instroomt nog steeds onveranderd is (ca. + 3 m TAW, Aqua Vision 12/2017).

Ebstream: Evenals de vorige meetcampagnes begint een kwartier na hoog water de ebstream. Het water stroomt het gebied uit met debieten van rond de $25 \text{ m}^3/\text{s}$. Er worden zeer grote variaties in de ebstream debieten gemeten zoals in eerdere campagnes ook het geval was, maar niet in de vorige campagne in juli 2018.

Getij asymmetrie: Voor de campagne in oktober 2018 geldt wederom dat de ebfase langer duurt dan de vloedfase. Dit wordt getijasymmetrie genoemd, waarbij de hoge vloedsnelheden t.o.v. ebsnelheden (op de lange termijn) zorgen voor verzanding.



Figuur 10: Getij en gemeten debiet op 23 oktober 2018. Negatief debiet duidt op vloedstroom, positief debiet duidt op ebstream.



Figuur 11: Getij en gemeten debiet op 11 juli 2018. Negatief debiet duidt op vloedstroom, positief debiet duidt op ebstream. In het paars debieten gemeten bij de ingang, noordzijde, van het gebied – niet aansluitend in de tijdreeks.

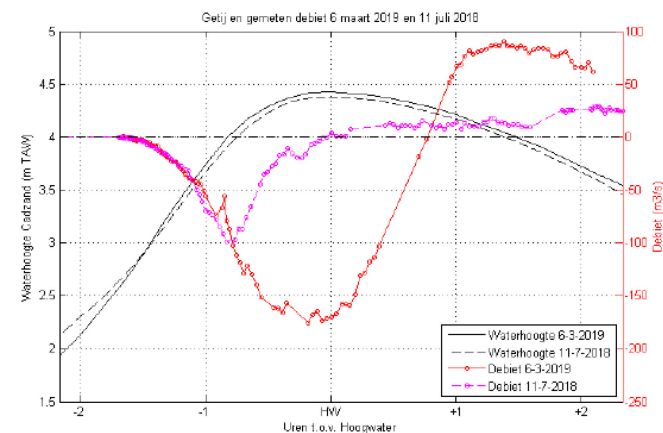
6/03/2019

Om debieten te bepalen door de hoofdgeul, zijn de bathymetrische meetraaien telkens dwars op de stroming gevaren. Het gebied is ingemeten vanuit de zeezijde, landinwaarts. De gemeten stromingsdata worden gefilterd (zodat het stroombeeld beter zichtbaar is) weergegeven in presentaties, welke zijn meegeleverd met deze rapportage. Uit de gemeten stroomsnelheidsdata zijn debieten berekend met behulp van ViSea. Figuur geeft het getij en gemeten debiet weer op 6 maart.

Vloedstroom: Op 6 maart 2019 is er een maximaal debiet van 175 m³/s gemeten, gedurende vloedfase. Uit de vergelijking met juli 2018 kan worden opgemaakt dat het karakter van de getijgolf in het Zwin is veranderd. Voor de opening toonde de golf karakteristieken van een “staande” golf (maximale vloedpiek op het moment van grootste waterstandsverschil). Doordat er meer komberging is gegenereerd stroomt er meer water het Zwin in. Echter, de grootte van de toegangsgeul is hier nog niet aangepast aan de grotere getijvolumes. Dit zorgt voor veel bodemwrijving waardoor de toegangsgeul groter wordt. Deze bodemwrijving zorgt voor een faseverschuiving van de getijdegolf waardoor deze meer het karakter krijgt van een “lopende” golf. De duur van de vloedstroom in maart 2019 was ongeveer 2u30, terwijl dit in juli 2018 nog 1u45 was. Het totale volume water wat met de vloedstroom binnen stroomde is berekend op 805.312 m³.

Ebstroom: De ebstroom begint drie kwartier na hoogwater en stijgt snel tot de maximale debieten van ongeveer 80 m³/s. Vervolgens daalt dit debiet zeer geleidelijk. In vergelijking met de meting in juli 2018 is de grote van het ebstroom debiet ongeveer verdrievoudigd.

Getij asymmetrie: Voor de campagne in maart 2019 geldt ondanks de gebiedsuitbreiding nog steeds dat de ebfase langer duurt dan de vloedfase. Het resultaat is van deze getijdeasymmetrie is dat de stroomsnelheden tijdens vloed groter zijn dan tijdens eb. Dit resulteert doorgaans in verzanding van het systeem. Door de dijkboorbraak en het daarmee vergroten van de komberging heeft er op dit moment een kleine verschuiving plaatsgevonden; het systeem is relatief minder vloeddominant geworden. De verwachting is echter dat (op de langere termijn en zonder ingrepen) verzanding van het systeem zal optreden. Dit zal hoofdzakelijk optreden (aan de zijkanten en het achterste deel van het gebied) daar waar de stroming minder geconcentreerd is en over korte afstand snel afneemt.



Figuur 9: Getij en gemeten debiet op 6 maart 2019 en 11 juli 2018. De debieten van juli 2018 op +2 uur na HW zijn gemeten bij de ingang, noordzijde, van het gebied – niet aansluitend in de tijdreeks.

<p>17,18/06/2019</p>	<p>Om debieten te bepalen door de hoofdgeul, zijn de bathymetrische meetraaien telkens dwars op de stroming gevaren. Het gebied is ingemeten vanuit de zeezijde, landinwaarts. De gemeten stromingsdata worden gefilterd (zodat het stroombeeld beter zichtbaar is) weergegeven in presentaties, welke zijn meegeleverd met deze rapportage. Uit de gemeten stroomsnelheidsdata zijn debieten berekend met behulp van ViSea. Figuur geeft het getij en gemeten debiet weer op 17 juni.</p> <p>Vloedstroom: Op 17 juni 2019 is er een maximaal debiet van 228 m³/s gemeten, gedurende vloedfase. Dit komt neer op een toename van ongeveer 30% ten opzichte van 6 maart 2019. Uit de vergelijking met maart 2019 kan worden opgemaakt dat het karakter van de getijgolf in het Zwin niet significant is veranderd. Voor de opening in februari 2019 toonde de golf karakteristieken van een "staande" golf (maximale vloedpiek op het moment van grootste waterstandsverschil). Doordat er meer komberging is gegeneerd stroomt er meer water het Zwin in. In maart 2019 was de grootte van de toegangsgoel nog niet aangepast aan de grotere getijvolumes. Dit zorgde voor veel bodemwrijving waardoor een faseverschuiving van de getijdegolf werd waargenomen. In juni 2019 is de toegangsgoel breder geworden en is de faseverschuiving kleiner geworden. De duur van de vloedstroom in juni 2019 was ongeveer 2u30, wat ongeveer gelijk is aan de duur van de vloedstroom van maart 2019. Het totale volume water wat met de vloedstroom binnenstroomde is berekend op 971.363 m³, terwijl dit in maart 2019 805.312 m³ was. Het totale volume is dus met zo'n 20% gestegen.</p> <p>Ebstroom: De ebstroom begint drie kwartier na hoogwater en stijgt snel tot het maximale debiet van ongeveer 116 m³/s, wat een toename is van meer dan 40% ten opzichte van 6 maart 2019. Vervolgens daalt dit debiet zeer geleidelijk.</p> <p>Getij asymmetrie: Voor de campagne in juni 2019 geldt dat de ebfase langer duurt dan de vloedfase. Het resultaat van deze getijdeasymmetrie is dat de stroomsnelheden tijdens vloed groter zijn dan tijdens eb. Dit resulteert doorgaans in verzanding van het systeem. De verwachting is dat (op de langere termijn en zonder ingrepen) verzanding van het systeem zal optreden. Dit zal hoofdzakelijk optreden (aan de zijkanten en het achterste deel van het gebied) daar waar de stroming minder geconcentreerd is en over korte afstand snel afneemt.</p>	<p>Figuur 9: Getij en gemeten debiet op 17 juni 2019 en 6 maart 2019.</p>
----------------------	---	---

<p>16,17/09/2019</p>	<p>Om debieten te bepalen door de hoofdgeul, zijn de bathymetrische meetraaien telkens dwars op de stroming gevaren. Het gebied is ingemeten vanuit de zeezijde, landinwaarts. De gemeten stromingsdata worden gefilterd (zodat het stroombeeld beter zichtbaar is) weergegeven in presentaties, welke zijn meegeleverd met deze rapportage.</p> <p>Uit de gemeten stroomsnelheidsdata zijn debieten berekend met behulp van ViSea. Figuur geeft het getij en gemeten debiet weer op 16 september. Vloedstroom: Op 16 september 2019 is er een maximaal debiet van 270 m³/s gemeten, gedurende vloedfase. Dit komt neer op een toename van 18% ten opzichte van 17 juni 2019. Uit de vergelijking met juni 2019 kan worden opgemaakt dat het karakter van de getijgolf in het Zwin niet significant is veranderd. De faseverschuiving (tussen getij en debiet, Aqua Vision 06/2019) is nagenoeg gelijk gebleven ten opzichte van juni 2019. De snelheid waarmee de toegangsecul verandert is afgenomen. Het systeem lijkt zich richting een nieuw evenwicht te begeven. De duur van de vloedstroom in september 2019 was ongeveer 2u30, wat ongeveer gelijk is aan de duur van de vloedstroom van maart en juni 2019. Het totale volume water wat met de vloedstroom binnenstroomde is berekend op 1,14 miljoen m³ ten opzichte van 0,97 miljoen m³ (toename van 17%).</p> <p>Ebstroom: De ebstroom begint ongeveer drie kwartier na hoogwater en stijgt snel tot het maximale debiet van ongeveer 140 m³/s, wat een toename is van 20% ten opzichte van 17 juni 2019. Dit debiet daalt relatief snel tot na 20 minuten een vergelijkbaar debiet als 17 juni 2019 wordt bereikt (rond de 100 m³/s). Vervolgens daalt dit debiet zeer geleidelijk.</p> <p>Getij asymmetrie: Ook voor de campagne in september 2019 geldt dat de ebfase langer duurt dan de vloedfase (evenals voorgaande campagnes). Het resultaat van deze getijdeasymmetrie is dat de stroomsnelheden tijdens vloed groter zijn dan tijdens eb. Dit resulteert doorgaans in verzanding van het systeem. De verwachting is dat (op de langere termijn en zonder ingrepen) verzanding van het systeem zal optreden. Dit zal hoofdzakelijk optreden (aan de zijkanten en het achterste deel van het gebied) daar waar de stroming minder geconcentreerd is en over korte afstand snel afneemt.</p>	<p>Figuur 8: Getij en gemeten debiet op 16 september 2019 en 17 juni 2019.</p>
----------------------	---	--

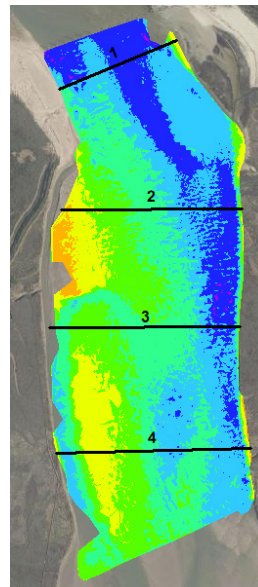
A. 4.List of Aqua Vision reports:

- Aqua Vision (2019) Het Zwin, bathymetrie en stromingsmetingen juli 2019. Report, 23pp.
- Aqua Vision (2019) Het Zwin, bathymetrie en stromingsmetingen juli 2019. Report, 25pp.
- Aqua Vision (2019) Het Zwin, bathymetrie en stromingsmetingen maart 2019. Report, 25pp.
- Aqua Vision (2019) Het Zwin, bathymetrie januari 2019. Report, 21pp.
- Aqua Vision (2018) Het Zwin, bathymetrie en stromingsmetingen oktober 2018. Report, 26pp.
- Aqua Vision (2018) Het Zwin, bathymetrie en stromingsmetingen juli 2018. Report, 29pp.
- Aqua Vision (2018) Het Zwin, bathymetrie en stromingsmetingen april 2018. Report, 29pp.
- Aqua Vision (2017) Het Zwin, bathymetrie en stromingsmetingen december 2017. Report, 185pp.
- Aqua Vision (2017) Het Zwin, bathymetrie en stromingsmetingen juli 2017. Report, 203pp.

Appendix B

Morphological characteristics of the inland inlet extracted from the profiles

Profile 1		Elevation (m)		
Survey	Period	Average	Maximum	Minimum
10-11/07/2017	Jul-17	2.39	3.00	1.92
18-19/12/2017	Dec-17	1.92	2.67	1.09
11-12-13/04/2018	Apr-18	1.68	2.37	0.77
10-11-12, 16/07/2018	Jul-18	2.33	4.09	1.14
23-24-25/10/2018	Oct-18	2.60	4.58	1.04
30/01-01/02/2019	Jan-19	2.33	3.47	1.21
06-07/03/2019	Mar-19	2.45	2.71	2.05
17-18/06/2019	Jun-19	2.14	2.52	1.69
16-17/09/2019	Sep-19	2.06	2.66	1.58



Profile 2		Elevation (m)		
Survey	Period	Average	Maximum	Minimum
10-11/07/2017	Jul-17	2.94	3.39	2.45
18-19/12/2017	Dec-17	3.00	3.82	2.46
11-12-13/04/2018	Apr-18	3.05	3.49	2.39
10-11-12, 16/07/2018	Jul-18	3.11	3.74	2.47
23-24-25/10/2018	Oct-18	3.18	3.60	2.50
30/01-01/02/2019	Jan-19	3.23	3.80	2.49
16-17/09/2019	Sep-19	3.26	4.03	1.43
17-18/06/2019	Jun-19	2.78	3.87	1.18
16-17/09/2019	Sep-19	2.76	4.03	1.43

Profile 3		Elevation (m)		
Survey	Period	Average	Maximum	Minimum
10-11/07/2017	Jul-17	2.93	3.53	2.59
18-19/12/2017	Dec-17	2.99	3.39	2.56
11-12-13/04/2018	Apr-18	2.97	3.42	2.35
10-11-12, 16/07/2018	Jul-18	3.07	3.51	2.39
23-24-25/10/2018	Oct-18	3.17	3.62	2.73
30/01-01/02/2019	Jan-19	3.21	3.77	2.69
06-07/03/2019	Mar-19	3.17	3.61	2.35
17-18/06/2019	Jun-19	2.68	3.40	2.03
16-17/09/2019	Sep-19	2.76	3.47	1.56

Profile 4		Elevation (m)		
Survey	Period	Average	Maximum	Minimum
10-11/07/2017	Jul-17	2.99	3.14	2.55
18-19/12/2017	Dec-17	3.08	3.32	2.44
11-12-13/04/2018	Apr-18	3.11	3.31	2.54
10-11-12, 16/07/2018	Jul-18	3.22	3.58	2.70
23-24-25/10/2018	Oct-18	3.34	4.22	2.47
30/01-01/02/2019	Jan-19	3.35	3.61	2.69
06-07/03/2019	Mar-19			
17-18/06/2019	Jun-19	2.90	3.64	2.04
16-17/09/2019	Sep-19	2.83	4.16	1.83

Appendix C

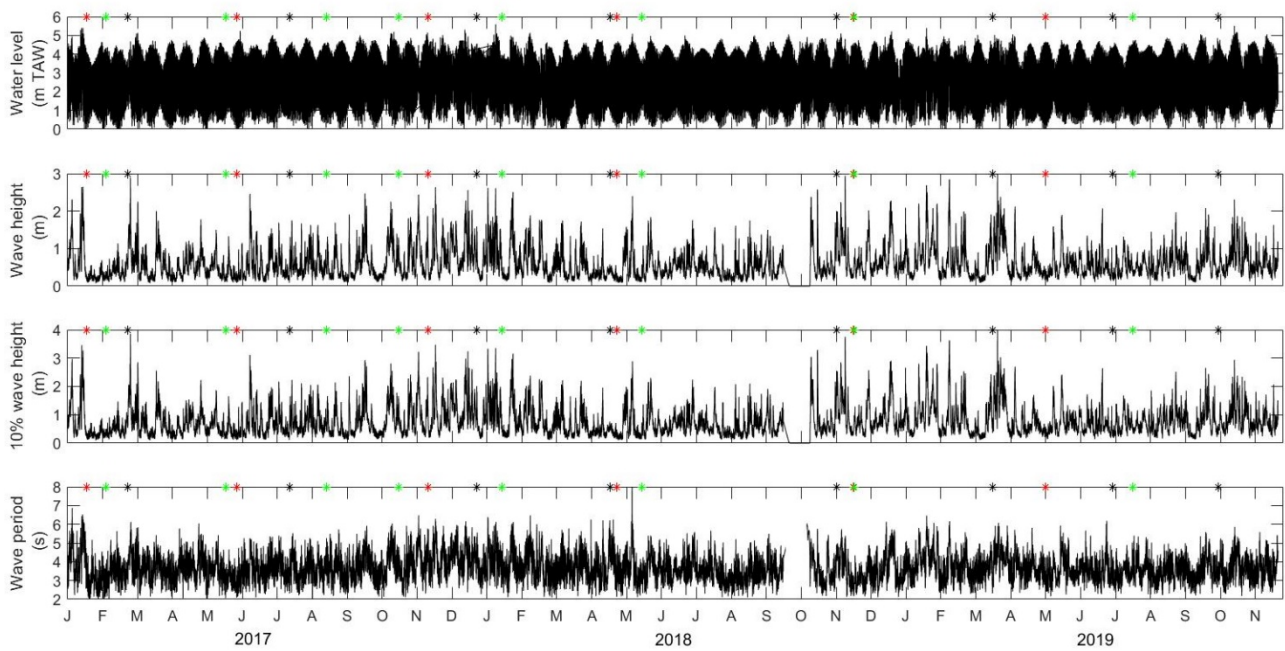
Locations of the continuous monitoring marine stations.



Appendix D

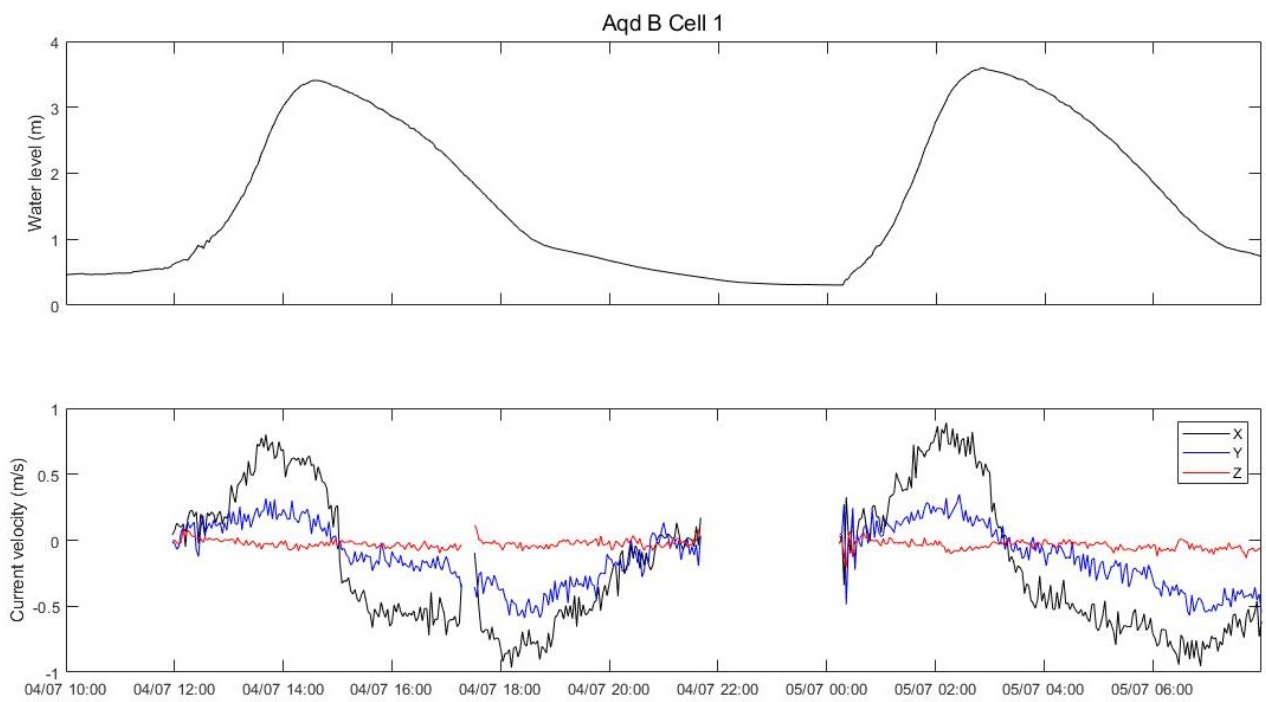
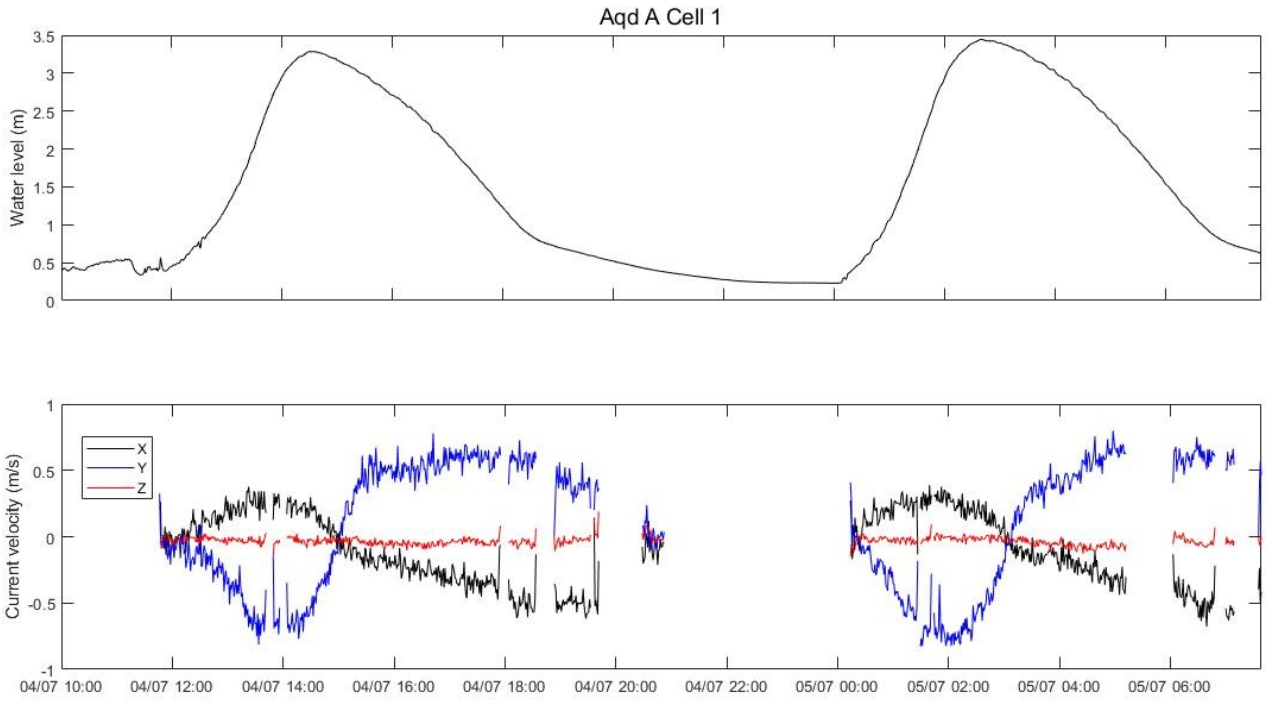
Time series of water level, average wave height, 10% wave height and wave period from Scheur.

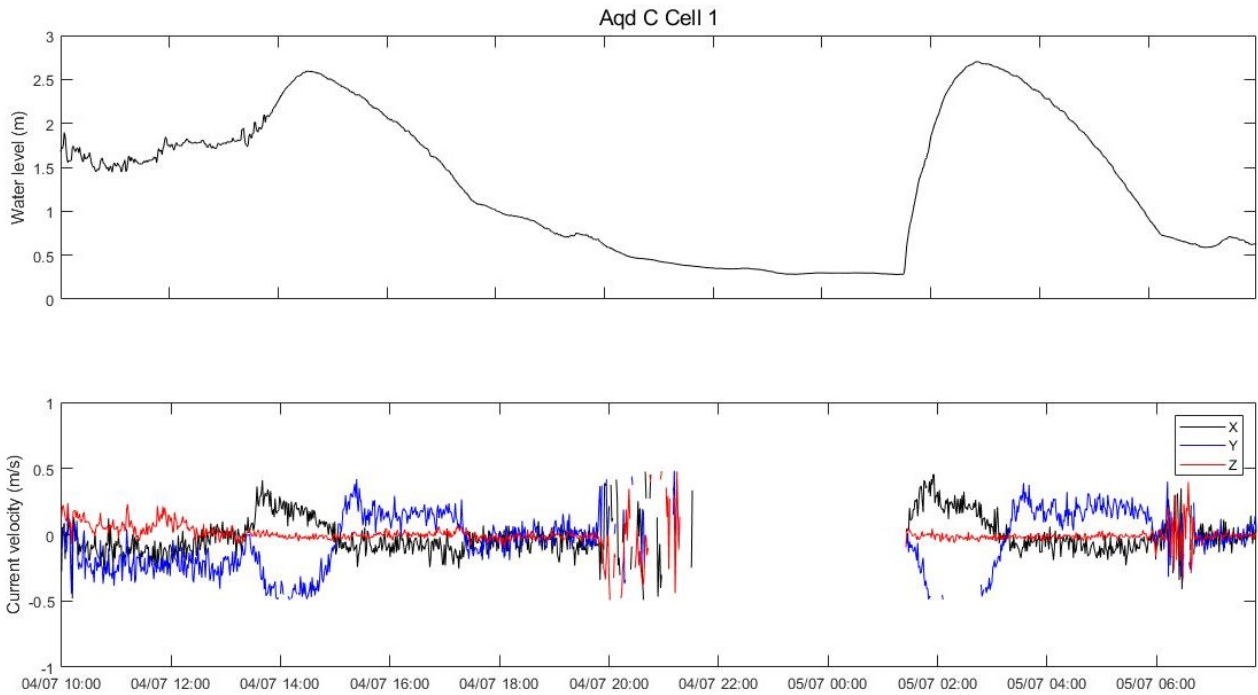
Missing water level data from 05/11/2017 to 26/10/2017 was filled up with records at Zeebrugge and wave parameters from 30/9/2018 to 28/11/2018 with Bol van Heist records. Red, green and black stars correspond to the LiDAR, RTK-GPS and Qboat surveys.



Appendix E

Comparison of current velocity for u, v and w components for cell 1





Bluk statistics of the current velocity for the three components recorded by the cell 1 of the 3 Aquadopps:

		Current Velocity (m/s)				
		Mean	Median	Max	Min	SD
Aqd A	X	-0.060	-0.083	0.389	-0.500	0.241
	Y	0.059	0.007	0.500	-0.500	0.311
	Z	-0.034	-0.034	0.190	-0.151	0.032
Aqd B	X	-0.185	-0.345	0.890	-0.965	0.511
	Y	-0.114	-0.116	0.348	-0.589	0.232
	Z	-0.032	-0.033	0.113	-0.207	0.035
Aqd C	X	-0.010	-0.037	0.476	-0.500	0.145
	Y	-0.040	-0.018	0.484	-0.493	0.210
	Z	0.002	-0.006	0.481	-0.494	0.085

DEPARTMENT **MOBILITY & PUBLIC WORKS**
Flanders hydraulics Research

Berchemlei 115, 2140 Antwerp

T +32 (0)3 224 60 35

F +32 (0)3 224 60 36

waterbouwkundiglabo@vlaanderen.be

www.flandershydraulicsresearch.be